Research Square

Preprints are preliminary reports that have not undergone peer review.
They should not be considered conclusive, used to inform clinical practice,
or referenced by the media as validated information.

Spatiotemporal Characterization of GSTO1 Inhibition in Postoperative Cognitive Dysfunction: Roles of Hippocampal Oxidative Stress and Neuroinflammation in Aged Mice

Guangwei Huang[1]
Zunyi Maternal and Child Health Care Hospital
Jing Li[2]
Affiliated Hospital of Zunyi Medical College
Hualiu Chen[3]
Guizhou Aerospace Hospital
Huanhuan Ma
20145762@qq.com
Guizhou Aerospace Hospital

Research Article

Keywords: GSTO1, Postoperative cognitive dysfunction, Oxidative stress, Neuroinflammation, Morris water maze

Posted Date: September 8th, 2026

DOI: https://doi.org/10.21203/rs.3.rs-10575974/v1

License: This work is licensed under a Creative Commons Attribution 4.0 International License.
Read Full License

Additional Declarations: No competing interests reported.

Version of Record: A version of this preprint was published at BMC Pharmacology and Toxicology on October 30th, 2026. See the published version at https://doi.org/10.1186/s40360-026-01270-5.

Spatiotemporal Characterization of GSTO1 Inhibition in Postoperative Cognitive Dysfunction: Roles of Hippocampal Oxidative Stress and Neuroinflammation in Aged Mice

Guangwei Huang[1], Jing Li[2], Hualiu Chen[3], Huanhuan Ma[3]*

1 Department of Anesthesiology, Zunyi Maternal and Child Health Care Hospital, Zunyi, Guizhou 563000, China
2 Department of Anesthesiology, Affiliated Hospital of Zunyi Medical University, Zunyi, Guizhou 563000, China
3 Department of Anesthesiology, Guizhou Aerospace Hospital, Zunyi, Guizhou 563000, China

Guangwei Huang and Jing Li are co-first authors.

*Corresponding author: Huanhuan Ma, Email: 20145762@qq.com

Abstract

Objective This preliminary study evaluated the time-dependent effects of hippocampal glutathione S-transferase omega 1 (GSTO1) inhibition on postoperative cognitive function, oxidative stress, and neuroinflammation in aged mice. **Methods** Seventy-two aged C57BL/6 mice were randomized into four groups (n=18/group): Surgery+C1-27, Surgery+Vehicle, C1-27 only, and Control. Following Morris water maze pre-training, the respective interventions were performed. Spatial memory, hippocampal GSTO1 expression level, oxidative stress markers (ROS, MDA, GSH/GSSG ratio), pro-inflammatory cytokines (TNF-α, IL-1β, IL-6), and amyloid precursor protein (APP) deposition were dynamically evaluated at 6 h, 3 d, and 7 d post-modeling. **Results** Pharmacological GSTO1 inhibition combined with surgical trauma induced an acute decline in hippocampal GSTO1 expression at 6 h, along with a marked reduction of the GSH/GSSG ratio ($P < 0.05$). The disrupted antioxidant system was accompanied by gradual increases in ROS, MDA and pro-inflammatory factors, as well as time-dependent APP deposition in the hippocampal CA1, CA3 and DG regions over the observational period. These cumulative microenvironmental injuries eventually led to obvious spatial memory deficits at postoperative day 3 and day 7 ($P < 0.05$). **Conclusion** Surgical trauma

and pharmacological GSTO1 inhibition drive a multi-phase pathological cascade characterized by acute impairment of hippocampal antioxidant defense, progressive neuroinflammation, and structural APP accumulation, which ultimately lead to exacerbated spatial memory deficits. These descriptive findings suggest that GSTO1-regulated microenvironmental homeostasis is critically involved in perioperative cognitive decline, establishing a foundation for future genetic causal validation.

Keywords: GSTO1; Postoperative cognitive dysfunction; Oxidative stress; Neuroinflammation; Morris water maze

1. Introduction

With the accelerating global aging process, the number of elderly patients undergoing surgical procedures under general anesthesia is steadily increasing. Consequently, perioperative neurocognitive disorders, particularly postoperative cognitive dysfunction (POCD), have become a major clinical concern. Clinically, POCD is characterized by postoperative memory decline, impaired abstract thinking, and disorientation, severely diminishing patients' quality of life and social integration. Although the exact etiology of POCD remains multifactorial and elusive, growing evidence demonstrates that an altered central microenvironment—characterized by the reciprocal aggravation of neuroinflammatory responses and oxidative stress—plays a foundational role in its pathogenesis(1, 2)

Glutathione S-transferase omega 1 (GSTO1), a novel member of the omega class of the glutathione S-transferase (GST) family, is widely recognized for its critical roles in maintaining cellular redox homeostasis, detoxification defense, and resistance to oxidative injury(3) . Genetic variants of GSTO1 have been closely linked to the susceptibility and onset age of neurodegenerative diseases characterized by cognitive decline, including Alzheimer’s disease and vascular dementia(4, 5). Within the central nervous system, GSTO1 is abundantly distributed in the hippocampus, a core anatomical region governing learning and memory processing(5). Given its unique ability to

modulate glutathione metabolism and eliminate reactive oxygen species, GSTO1 is considered a potential sentinel against microenvironmental stress in the brain.

Intriguingly, our previous clinical serum proteomic study on patients undergoing cardiac valve replacement surgery first identified that GSTO1 and several redox-related proteins were significantly downregulated in patients who developed POCD, with their expression levels negatively correlating with postoperative cognitive scores(6). This clinical clue strongly implies that GSTO1 deficiency may participate in the pathological progression of perioperative cognitive decline. However, due to the inherent constraints of clinical sampling, whether and how local suppression of GSTO1 within the hippocampus dynamically influences the temporal progression of cognitive function, oxidative status, and neuroinflammation remains to be elucidated.

Therefore, as a crucial translational step following our clinical findings, the present study established an aged mouse model to systematically evaluate the temporal dynamics of pharmacological GSTO1 inhibition in the hippocampus. To establish a comprehensive foundational baseline before undertaking targeted genetic manipulations, this study focuses on capturing the sequential, longitudinal alterations (at 6h, 3d, and 7d) in spatial memory, redox balance, inflammatory cytokine profiles, and pathological protein accumulation following GSTO1 suppression. By shifting the perspective toward a temporal microenvironmental profile, this longitudinal characterization aims to provide definitive in vivo evidence regarding the dynamic role of GSTO1 in perioperative neurological homeostasis.

2. Materials and Methods

2.1 Experimental Animals and Grouping

A total of 72 male C57BL/6 mice (12–14 months old, 30–37 g) were purchased from Jiangsu Huachuang Sino Pharmaceutical Technology Co., Ltd. (License No. SCXK (Su) 2020-0009). The mice were acclimated under specific pathogen-free (SPF) conditions (50–60% humidity, 20–24°C, 12 h light/dark cycle) with ad libitum access to water and food. To minimize baseline experimental variance driven by cyclic estrous hormonal

fluctuations in neuroinflammatory and oxidative pathways(7), only male mice were selected for this foundational temporal profiling study.

An a priori sample size calculation was performed using G*Power software (version 3.1.9.7). Based on prior literature and preliminary evaluations of perioperative neuroinflammation, an effect size $f = 0.40$, a significance level $\alpha = 0.05$, and a power $(1 - \beta) = 0.80$ dictated a required sample size of $n = 6$ per cohort for distinct longitudinal biochemical time points, and a cumulative $n = 18$ per main group to robustly evaluate overlapping behavioral phenotypes.

Using a computer-generated random number sequence, mice were assigned to a 2×2 fully crossed factorial experimental layout consisting of four standardized cohorts ($n = 18$ per group):

1. **Control (Sham+Vehicle) group:** Underwent time-matched anesthesia (140 min total), stereotaxic needle insertion, and 10% (v/v) dimethyl sulfoxide (DMSO) microinjection to establish a baseline independent of surgical trauma.
2. **C1-27 group:** Underwent time-matched anesthesia (140 min total), stereotaxic needle insertion, and specific GSTO1 inhibitor C1-27 microinjection to isolate target-specific intrinsic effects.
3. **Surgery+Vehicle group:** Underwent a 140-minute surgical intervention (exploratory laparotomy) paired with hippocampal 10% DMSO microinjection to isolate surgical trauma stress.
4. **Surgery+C1-27 group:** Underwent a 140-minute surgical intervention (exploratory laparotomy) paired with hippocampal C1-27 microinjection to evaluate the synergistic impact of surgery and target inhibition.

All animal housing, handling, and surgical interventions were strictly approved by the Animal Ethics Committee of Zunyi Medical University (Approval No. ZMU21-2207-008) and meticulously complied with the National Guidelines for Laboratory Animal Management.

2.2 Main Reagents and Equipment

The specific, small-molecule covalent GSTO1 inhibitor C1-27 (Cat. No. HY-111530) was obtained from MedChemExpress (MCE). Isoflurane (Cat. No. R510-22-10) was procured from Shenzhen RWD Life Science Co. The rabbit anti-GSTO1 primary antibody (Cat. No. A15354) was purchased from ABclonal Technology. The rabbit anti-TNF-α(Cat. No. 60291-1-Ig) and rabbit anti-APP (Cat. No. 25524-1-AP) primary antibodies were acquired from Wuhan Sanying Biotechnology (Proteintech). HRP-conjugated goat anti-rabbit secondary antibody (Cat. No. A0208) was from Beyotime Biotechnology. PVDF membranes (0.45 μm, Cat. No. IPVH00010) were obtained from Millipore. Commercially validated ELISA kits for GSH (Cat. No. KTB1600-96T) and GSSG (Cat. No. KTB1610) were from Abbkine. High-sensitivity ELISA kits for ROS (Cat. No. MM-43700M1), IL-6 (Cat. No. MM-0163M1), and IL-1β (Cat. No. MM-0040M2) were obtained from Jiangsu Meimian Industrial Co.

The Morris water maze apparatus, tracking software, stereotaxic coordinates frame, and automated microinjection pumps were maintained by the Key Laboratory of Anesthesia and Organ Protection of Guizhou Province. Absorbance data were resolved using an automatic microplate reader (Thermo iSKAN MK3), and electrophoretic sorting was conducted via a Liuyi DYCZ-40 apparatus.

2.3 Experimental Methods

2.3.1 Pharmacological Dose Optimization: Cell-Free IC_{50} vs. In Vivo EC_{50}

In vitro assays have determined that C1-27 exerts an inhibitory effect on purified GSTO1 with an IC_{50} of 31 nM (8). Given the distinct physiological microenvironment of brain tissue, we performed an in vivo dose-gradient experiment to screen the optimal working concentration of C1-27. After stereotactic injection into the hippocampal CA1 region, small-molecule agents need to overcome multiple biological barriers, including interstitial fluid diffusion, non-specific binding to extracellular matrix components and in situ metabolic clearance (9, 10).

A series of C1-27 solutions with concentrations ranging from 310 nM to 31 mM were prepared using 10% DMSO diluted with sterile saline. The prepared agents were

bilaterally injected into the hippocampal CA1 region at a total volume of 1.2 μL per mouse. Hippocampal tissues were harvested 6 h after administration, and Western blot was used to detect GSTO1 protein expression. A four-parameter logistic (4PL) regression model was applied to calculate the in vivo half-maximal effective concentration (EC_{50}) of C1-27 for GSTO1 suppression(11).

2.3.2 Morris Water Maze (MWM) Behavioral Assay

To capture spatial learning and memory profiles, mice underwent a standardized MWM paradigm following protocols optimized for aging-induced cognitive tracking(12, 13) . The setup comprised a circular pool (120 cm diameter, 60 cm height) filled with opaque water (24~26℃) under a muted acoustic environment. A stationary cylindrical escape platform (15 cm diameter, 30 cm height) was submerged 1 cm below the surface in a designated target quadrant.

For 5 consecutive days prior to surgical/pharmacological modeling, mice received baseline place navigation training consisting of four trials per day (one per starting quadrant, randomized daily). In each trial, the mouse was released facing the pool wall and allotted 60 s to locate the hidden platform. If successful, it remained on the platform for 10s; if it failed within 60s, it was manually guided to the platform and allowed to adjust for 10s, yielding an escape latency score of 60s. On the afternoon of training day 5, a spatial probe trial (platform removed) was executed to confirm spatial baseline competency. Following modeling, longitudinal spatial memory retention was tracked via subsequent probe trials performed at post-modeling day 3 and day 7.

To guarantee behavioral data integrity and eliminate potential physiological confounders, strict animal selection and exclusion rules were enforced:

- Mice exhibiting congenital visual deficits, severe persistent floating behavior, or profound thigmotaxis (wall-hugging exceeding 85% of total swimming duration) during the initial training phase were excluded.
- Average swimming velocity was calculated for every trial; mice displaying a mean swim speed below 0.1m/s were classified as possessing gross locomotor or

motor-sensory impairments independent of cognitive state and were excluded from cognitive evaluation(14, 15) .

- All behavioral trials, video tracking acquisition, and subsequent path parameters were automated and analyzed by investigators entirely blinded to the animal grouping assignments.

2.3.3 Surgical Modeling and Synchronized Anesthesia Protocol

The POCD model was established via exploratory laparotomy as previously described (16). To distinguish the effects of surgical trauma and volatile anesthetics, the total duration of isoflurane exposure was strictly unified across all four groups. Anesthesia was induced with 4% isoflurane and maintained at 2% in 100% oxygen.

For Surgery+Vehicle and Surgery+C1-27 groups, the 140-minute protocol consisted of a 20-minute abdominal incision and layered closure, followed by 120 minutes of gentle abdominal organ exploration to induce surgical stress. After that bilateral hippocampal microinjection was performed.

Control and C1-27 groups received only scalp incision and hippocampal injection without abdominal surgery. Their isoflurane inhalation was prolonged to reach a total exposure of 140 min. Core body temperature was maintained at 37±0.5 °C throughout the study to avoid hypothermia-induced neuroinflammation.

2.3.4 Collection of Hippocampal Tissue

At designated temporal milestones (6 h, 3 d, and 7 d post-modeling), 6 mice were randomly selected from each group using a random-number table. Following deep surgical anaesthesia via intra-peritoneal injection of 1% pentobarbital sodium (50 mg/kg), mice were humanely euthanized with an additional intra-peritoneal overdose of pentobarbital sodium (200 mg/kg). Complete loss of the pedal-withdrawal reflex and corneal reflex was confirmed to verify full unconsciousness prior to tissue harvesting, in accordance with AVMA Guidelines for the Humane Euthanasia of Laboratory Animals. Immediately after euthanasia, mice were rapidly decapitated under aseptic conditions; intact brains were dissected on an ice-chilled platform. Hippocampal formations were carefully isolated, transferred into sterile 1.5 mL microcentrifuge tubes, and instantly

snap-frozen in liquid nitrogen for long-term storage at -80 ℃ For histological/morphological cohorts, mice underwent transcardial perfusion-fixation as described below.

2.3.5 Western Blot Analysis of Hippocampal GSTO1

Hippocampal tissues were homogenized in pre-cooled lysis buffer containing 1% PMSF (300 μL per sample) using a tissue homogenizer with steel beads. After incubation on ice for 30 min, lysates were centrifuged at 12,000 r/min and 4 °C for 5 min. Protein concentration of the supernatant was determined via BCA assay.

Total protein (30 μg) was denatured at 100 °C for 10 min, then separated by SDS-PAGE (5% stacking gel, 12% separating gel; 80 V initially, then 120 V for approximately 1.5 h) and transferred onto methanol-activated PVDF membranes at 200 mA for 90 min. Membranes were cut according to protein molecular weight markers for separate incubation of target protein and internal control.

After blocking with 5% skim milk in TBST for 2 h at room temperature, membranes were incubated overnight at 4 °C with primary antibodies against GSTO1 (1:1000) and GAPDH (1:2000). Following five washes (5 min each) with TBST, blots were incubated with HRP-conjugated secondary antibody (1:600) for 2 h at room temperature. Protein bands were visualized using ECL reagent and imaged. Band density was quantified with ImageJ software, and GAPDH was used as the loading control.

2.3.6 ELISA Assays for Biochemical and Oxidative Stress Validation

Commercially available ELISA kits were used to detect hippocampal levels of GSH, GSSG, ROS, MDA, IL-1β and IL-6. All assays were performed in duplicate following the manufacturer's instructions. Standard curves were prepared with a correlation coefficient $R^2 > 0.99$.

2.3.7 Quantitative Immunofluorescence (IF) Analysis

Mice were perfused transcardially with ice-cold PBS followed by 4% paraformaldehyde (PFA). Isolated brain tissues were fixed in 4% PFA for 24 h, dehydrated and embedded in paraffin. Coronal sections (5 μm) of the dorsal hippocampus were prepared. Sections were deparaffinized and rehydrated, followed by antigen retrieval using sodium citrate

buffer (pH 6.0) via microwave heating for 20 min.

Endogenous peroxidase was inactivated with 3% H_2O_2, and non-specific binding was blocked with 5% BSA. Sections were incubated overnight at 4 °C with primary antibodies against GSTO1 and TNF-α (both 1:1000). Sections incubated only with secondary antibodies were set as negative controls. After PBS washing, sections were incubated with fluorophore-conjugated secondary antibody (1:500) for 60 min, and nuclei were counterstained with DAPI. Sections were mounted and imaged under a fluorescence microscope with unified exposure settings.

Image analysis was performed by two blinded investigators using ImageJ software. Three to four non-overlapping sections per mouse were analyzed. ROIs were defined for the CA1, CA3 and DG regions according to brain anatomical landmarks. Background fluorescence from the corpus callosum was subtracted, and results were presented as average optical density (AOD). Raw data were used for subsequent statistical analysis.

2.3.8 Quantitative Immunohistochemical (IHC) Assessment of APP

Paraffin sections were deparaffinized, rehydrated and subjected to antigen retrieval using citrate buffer as described above. After blocking, sections were incubated with anti-APP primary antibody (1:1000) overnight at 4 °C. Biotinylated secondary antibody and ABC detection system were applied sequentially for signal amplification. DAB was used for color development, and the reaction was stopped at a uniform contrast. Sections were counterstained with hematoxylin, dehydrated, cleared and mounted.

APP expression was quantified by ImageJ software. Fixed thresholds were applied to all sections for consistent signal extraction. ROIs were selected for hippocampal subfields, and staining intensity was calculated as AOD. Raw values were collected for statistical analysis.

2.3.9 Statistical Analysis and Comprehensive Parameters Reporting

All quantitative data are expressed as the mean ± standard deviation (SD). Prior to parametric statistical analyses, data normality was systematically verified using the Shapiro-Wilk test, and the homogeneity of variance was assessed using Levene's test. The escape latency during the 5-day navigation training was analyzed using a two-way repeated-measures ANOVA, with group as the between-subjects factor and training day

as the within-subjects factor. For spatial probe tests and subsequent histological and biochemical analyses (including IHC, IF, and ELISA), data at each specific time point were analyzed independently using a one-way ANOVA followed by Tukey's post-hoc test for multiple comparisons. Statistical analyses were performed using SPSS software (version 29.0; IBM Corp., Armonk, NY, USA). *P*-value < 0.05 was considered statistically significant.

3. Results

3.1 Optimization of Pharmacological Intervention and Verification of Microinjection Accuracy

(1) Verification of Hippocampal Targeting

Hippocampal injection accuracy was anatomically validated using the retrograde tracer cholera toxin B (CTB). Three days after microinjection, specific fluorescent signals were detected in the hippocampal CA1 and dentate gyrus (DG) regions, confirming the accuracy of the stereotactic coordinates (AP = -2.0 mm, ML = ±1.5 mm, DV = -1.6 mm) (Figure 1). These results verified precise targeting of all hippocampal pharmacological interventions.

(2) Dose-Response Optimization of C1-27

A dose-escalation assay was performed to determine the optimal in vivo concentration for hippocampal GSTO1 suppression, given that in vitro enzymatic IC_{50} values cannot fully recapitulate the complex microenvironment of the central nervous system. A gradient of C1-27 concentrations ranging from 310 nM to 62 mM was administered via hippocampal microinjection, and GSTO1 inhibitory efficiency was detected by Western blotting at 6 h post-injection (Table 1, Figure 2). Dose-dependent inhibitory effects of C1-27 on GSTO1 expression levels were further quantified via ELISA (Table 2, Figure 3), with inhibition rates ranging from 16% to 78% and exhibiting a sigmoidal dose-response relationship.

The dose-response data were fitted with a four-parameter logistic (4PL) regression model to calculate the in vivo half-maximal effective concentration (EC_{50}) of C1-27. The calculated EC_{50} was 3.405 mM (Figure 3). Combined with Western blot verification and

regression fitting results, 3.4 mM was selected as the optimal working concentration for all subsequent in vivo interventions.

Crucially, this optimized dose did not cause obvious damage to the histological structure of the hippocampal CA1 region, and no animal death was observed throughout the experiment. Meanwhile, the baseline total swimming distance was comparable across all groups (Figure 4B), confirming that this concentration did not affect the general locomotor ability of mice.

3.2 Longitudinal Assessment of Anesthetic Exposure and Spatial Memory Function

(1) Baseline Consistency of Anesthesia and Cognitive Learning

Total isoflurane exposure duration was standardized and compared across all experimental groups to eliminate anesthetic confounding factors, showing no significant intergroup differences (Control: 140.5 ± 1.8 min; C1-27: 139.8 ± 2.0 min; Surgery+Vehicle: 141.2 ± 1.5 min; Surgery+C1-27: 140.3 ± 2.2 min; $P > 0.05$)(Table S1 in Supplementary file).

During the 5-day spatial acquisition phase, two-way repeated-measures ANOVA revealed a significant main effect of training time on escape latency ($F(4, 272) = 154.597$, $P < 0.001$), indicating consistent learning improvement across all groups (Figure 4A). No significant main effect of group ($F(3, 68) = 1.910$, $P = 0.136$) or group × time interaction ($F(12, 272) = 0.971$, $P = 0.477$) was observed(Table S2 in Supplementary file). In addition, total swimming distance was comparable among all cohorts during baseline training ($P > 0.05$, Figure 4B). These findings confirmed consistent baseline learning ability and locomotor activity across groups, excluding pre-existing behavioral bias before surgical and pharmacological treatment.

(2) Postoperative Alterations in Spatial Memory Retention

Spatial memory retention was assessed at baseline, 3 and 7 days after modeling, with one-way ANOVA used for statistical analysis at each time point. For platform crossings (Figure 5A), no significant intergroup difference was observed at baseline ($F(3, 68) = 2.545$, $P = 0.063$). Significant differences were detected at postoperative day 3 ($F(3, 44)$

= 10.733, $P < 0.001$) and day 7 (F(3, 20) = 12.000, $P < 0.001$)(Table S3 in Supplementary file).

Consistent patterns were observed for the distance percentage (Figure 5B) and time percentage (Figure 5C) in the target quadrant. No baseline differences were detected for either index (distance percentage: F(3, 68) = 1.852, $P = 0.146$; time percentage: F(3, 68) = 1.225, $P = 0.307$). Following surgery, robust intergroup variations were identified at both postoperative milestones (postoperative day 3: all $P < 0.001$; day 7: distance percentage $P = 0.002$, time percentage $P < 0.001$)(Table S3 in Supplementary file).

(3) GSTO1 Suppression Aggravates Surgical Cognitive Impairment

Tukey's post-hoc multiple comparisons were performed to identify pairwise differences based on one-way ANOVA results (Figure 5). Compared with the Control group, the Surgery+Vehicle group showed significant reductions in platform crossings and target quadrant occupancy at postoperative day 3 and day 7, confirming successful establishment of the POCD model. The Surgery+C1-27 group exhibited further aggravated spatial memory deficits relative to the Surgery+Vehicle group at both time points (all $P < 0.05$). Mice treated with C1-27 alone also developed mild but significant spatial memory impairment, yet the cognitive damage was less severe than that caused by surgical trauma. Collectively, these findings indicate that GSTO1 inhibition independently impairs spatial memory and produces a synergistic effect with surgical stress to worsen POCD.

3.3 GSTO1 Inhibition Induces Sustained Hippocampal Redox Imbalance

(1) Effective and Sustained GSTO1 Suppression

GSTO1 expression was quantified by Western blot across three time points (Figure 6A, 6B). One-way ANOVA showed significant overall differences among groups at 6 h, 3 days and 7 days post-modeling (all $P < 0.001$). Post-hoc Tukey tests indicated that C1-27 treatment alone, surgical trauma, and their combination all significantly downregulated GSTO1 at 6 h. From day 3 to day 7, GSTO1 expression partially recovered. Significant downregulation relative to the Control group was only detected in the Surgery+Vehicle

group, while C1-27 monotherapy and the combined intervention produced no statistically significant effects at these later time points.

(2) Acute Oxidative Stress Burst Triggered by GSTO1 Deficiency

GSTO1 suppression triggered immediate and persistent hippocampal redox imbalance. All oxidative stress indicators showed significant intergroup differences at 6 h, 3 days, and 7 days after modeling (one-way ANOVA, all $P < 0.01$). Specifically, antioxidant capacity was significantly impaired, as reflected by reduced GSH levels (Figure 7A) and elevated GSSG levels (Figure 7B), leading to a sharp decline in the GSH/GSSG ratio (Figure 7C). Consistently, lipid peroxidation product MDA (Figure 7D) and ROS accumulation (Figure 7E) were markedly increased in the intervention groups at all time points. Post-hoc analysis further confirmed that the Surgery+C1-27 group exhibited the most pronounced oxidative imbalance, indicating that GSTO1 inhibition severely compromises the hippocampal antioxidant defense system and exacerbates surgery-induced redox imbalance.

3.4 GSTO1 Suppression Accelerates Acute and Persistent Neuroinflammation

Given the tight association between oxidative stress and neuroinflammation, hippocampal TNF-α expression was detected via immunofluorescence to evaluate neuroinflammatory responses (Figure 8A,Table 3 in Supplementary file).

One-way ANOVA detected significant intergroup differences in hippocampal TNF-α fluorescence intensity starting at 6 h post-modeling ($F(3, 20) = 3.123$, $P = 0.049$), with markedly amplified group disparities at postoperative day 3 ($F(3, 20) = 10.386$, $P < 0.001$) and day 7 ($F(3, 20) = 57.991$, $P < 0.001$). Tukey's post-hoc comparisons further revealed that TNF-α expression was significantly elevated in the C1-27 and Surgery+C1-27 groups relative to the Control group at all three time points, showing progressive exacerbation from 6 h to day 7.

3.5 Spatiotemporal Heterogeneity of Hippocampal APP Pathological Accumulation

To explore whether GSTO1 inhibition-induced microenvironmental disturbance drives neurodegenerative pathological changes, we detected APP expression in hippocampal

CA1, CA3, and DG subregions (Figure 9A–9C) and analyzed spatiotemporal pathological characteristics via one-way ANOVA.

In the CA1 region (Figure 9D), APP expression showed no significant intergroup difference at the acute 6 h stage ($F(3, 20) = 0.487$, $P = 0.695$). In contrast, significant APP upregulation emerged at 3 and 7 days post-operation (3 d: $F(3, 20) = 9.544$, $P < 0.001$; 7 d: $F(3, 20) = 32.285$, $P < 0.001$), with the highest expression observed in the Surgery+C1-27 group.

The CA3 and DG subregions exhibited earlier pathological responses. In the CA3 region (Figure 9E), significant intergroup differences in APP deposition were detected at 6 h ($F(3, 20) = 9.501$, $P < 0.001$) and persisted through 3 days ($P = 0.010$) and 7 days post-operation ($P < 0.001$). Similarly, the DG region showed obvious APP accumulation at the acute 6 h time point ($F(3, 20) = 5.332$, $P = 0.007$), with progressive pathological exacerbation at 3 and 7 days post-operation (all $P < 0.001$).

These subregion-specific differences indicated heterogeneous vulnerability of hippocampal subfields to surgical injury and GSTO1 suppression. Collectively, GSTO1 inhibition accelerates and exacerbates hippocampal APP accumulation, with the CA3 and DG subregions demonstrating greater sensitivity to early pathological damage than the CA1 region.

4. Discussion

4.1 Core Spatiotemporal Pathological Cascade Linking GSTO1 Inhibition to POCD

Postoperative neurocognitive dysfunction (POCD) predominantly affects elderly patients and represents a major perioperative neurological complication driven by excessive oxidative stress and sustained neuroinflammation in the hippocampus (1). Accumulating evidence has identified glutathione S-transferase omega 1 (GSTO1) as a pivotal antioxidant enzyme that maintains intracellular redox homeostasis and modulates inflammatory signaling across the central nervous system (CNS) (17, 18). Prior clinical proteomic work from our team demonstrated altered serum GSTO1 levels in patients experiencing perioperative cognitive impairment, implying a potential link between GSTO1 dysregulation and POCD progression (6). Nevertheless, direct in vivo evidence

clarifying how hippocampal GSTO1 dysfunction participates in POCD remains limited, and its spatiotemporal characteristics after surgical and pharmacological intervention have not been fully delineated.

In the current study using aged mice, we established a standardized POCD model combined with targeted hippocampal microinjection of the specific GSTO1 inhibitor C1-27. We first verified the accuracy of stereotaxic coordinates via cholera toxin B (CTB) tracing and optimized the in vivo working concentration of C1-27 through a series of dose-gradient experiments. Consistent with the pharmacological consensus that small-molecule agents encounter multiple diffusion and metabolic barriers in brain tissue(18), the in vivo EC_{50} of C1-27 (3.405 mM) was markedly higher than its in vitro IC_{50}, and the selected optimal dose exerted no obvious histological damage or locomotor disturbance, guaranteeing the reliability of subsequent phenotypic detection. All groups received strictly unified isoflurane exposure and preoperative behavioral training, eliminating anesthetic and baseline cognitive confounding factors.

Based on longitudinal observations at 6 h, 3 d and 7 d post-modeling, we systematically constructed a three-stage spatiotemporal pathological cascade triggered by hippocampal GSTO1 suppression: (1) The acute phase (6 h) is characterized by rapid GSTO1 downregulation and an abrupt redox collapse, manifested as decreased GSH/GSSG ratio and robust accumulation of ROS and MDA; (2) The subacute to chronic phase (3–7 d) witnesses progressive amplification of neuroinflammation represented by elevated TNF-α; (3) The late stage presents subfield-specific amyloid precursor protein (APP) deposition in the hippocampus, accompanied by irreversible spatial memory deficits. This sequential pathological progression closely matches the core pathogenic framework of perioperative neurocognitive disorders proposed in previous mechanistic reviews(19, 20), and first study to dynamically profile the sequential pathological alterations triggered by GSTO1 suppression in aged mice subjected to surgical trauma and anesthesia, providing original phenotypic evidence for the association between GSTO1 dysfunction and POCD progression.

4.2 GSTO1 Suppression Triggers Acute Hippocampal Redox Imbalance

As a redox-sensitive enzyme relying on the catalytic Cys112 residue, GSTO1 exerts core antioxidant functions via GSH-dependent disulfide reduction and thiol transferase activity, protecting neurons from oxidative damage(18, 21). In this study, both single C1-27 intervention and combined surgical trauma significantly reduced hippocampal GSTO1 expression at 6 h post-modeling, accompanied by an immediate burst of oxidative stress. The significant decline in reduced GSH levels, elevation of oxidized GSSG, and massive accumulation of ROS and MDA collectively indicated a comprehensive breakdown of the local antioxidant defense system. This finding is consistent with the view that GSTO1 is a key defender of CNS redox homeostasis(22).

Notably, partial spontaneous recovery of GSTO1 expression was observed at 3 d and 7 d after C1-27 treatment alone, with no significant difference compared with the control group at the two later time points. This compensatory response may be attributed to the adaptive feedback regulation of antioxidant pathways such as Nrf2 under mild oxidative stimulation(22). Nrf2 is the master transcription factor for antioxidant systems, and oxidative stress induced by short-term GSTO1 inhibition can activate the Nrf2-ARE axis to upregulate antioxidant proteins including GSTO1, forming a self-repair loop (23). In contrast, GSTO1 expression in the Surgery+Vehicle group remained persistently suppressed, suggesting that continuous systemic stress caused by surgical trauma can sustain the inhibition of hippocampal GSTO1 and block this compensatory recovery mechanism.

Our data also revealed that combined surgical trauma and C1-27 treatment led to the most severe redox disorder. This synergistic effect can be explained by the mutual reinforcement between surgical stress and GSTO1 dysfunction: surgery induces widespread systemic oxidative stress(24), while GSTO1 inhibition further weakens the hippocampus's ability to clear reactive oxygen species, ultimately forming a vicious cycle of oxidative damage. Distinct from chronic neurodegenerative diseases where GSTO1 often presents compensatory upregulation (25), the acute reduction of GSTO1 in our POCD model reflects the unique pathological feature of acute perioperative stress, which rapidly exhausts the brain's endogenous antioxidant reserves (6).

4.3 Temporal Coupling Between Oxidative Stress and Neuroinflammation Mediated by GSTO1

Oxidative stress and neuroinflammation are two inseparable core pathological links in perioperative neural injury, and GSTO1 acts as an important molecular bridge connecting the two processes (26, 27). In the present study, TNF-α, a classic pro-inflammatory cytokine, showed a unique temporal expression pattern: a marginal but statistically significant increase was detected as early as 6 h after modeling, and the inflammatory response continued to intensify at 3 d and 7 d, showing an obvious time lag relative to the acute oxidative burst. This chronological lag verifies the hypothesis that oxidative stress serves as an early trigger to drive sustained neuroinflammation in the hippocampus(19).

Mechanistically, GSTO1 functions as a critical deglutathionylase to regulate the activation of inflammatory cascades such as NLRP3 inflammasome and NF-κB signaling (26, 28). It specifically removes glutathione modifications on key inflammatory proteins (e.g., NEK7, NPM1) to modulate the assembly and transcriptional activity of inflammatory complexes. When GSTO1 is inhibited, this regulatory mechanism is impaired, and inflammatory signaling pathways are locked in a hyperactive state. In our model, acute ROS accumulation induced by GSTO1 suppression first disrupts neuronal homeostasis, then activates resident microglia and astrocytes, and further promotes the secretion of pro-inflammatory cytokines such as TNF-α(29). Long-term exposure to inflammatory factors in turn exacerbates oxidative stress, forming a persistent inflammatory-oxidative vicious circle.

Both single C1-27 treatment and combined intervention significantly upregulated hippocampal TNF-α expression throughout the observation period, demonstrating that GSTO1 inhibition alone is sufficient to initiate neuroinflammation. Meanwhile, the most prominent inflammatory response in the Surgery+C1-27 group further confirms that surgical trauma can amplify GSTO1-related inflammatory activation. This result is in line with previous reports that surgical stress activates peripheral and central inflammatory pathways (30), and combined with GSTO1 dysfunction, it profoundly aggravates hippocampal microenvironmental disorders. The dual regulatory role of GSTO1 on

oxidation and inflammation fully explains why its inhibition can independently induce cognitive impairment and synergistically exacerbate surgery-induced POCD.

4.4 Spatiotemporal Heterogeneity of Hippocampal APP Deposition and Pathological Implications

The hippocampus is a heterogeneous brain region composed of CA1, CA3 and dentate gyrus (DG) subfields, and different subregions exhibit distinct vulnerability to stress stimulation(31). In this study, we observed obvious spatiotemporal differences in APP accumulation across hippocampal subfields after GSTO1 inhibition and surgical intervention. APP is a key protein closely associated with neuronal damage and neurodegenerative lesions (5). In the CA1 region, no significant APP change was found at the acute 6 h stage, and obvious pathological deposition only appeared at 3 d and 7 d; by contrast, CA3 and DG showed significant APP upregulation as early as 6 h post-modeling, with continuous aggravation over time.

This subregional heterogeneity indicates that CA3 and DG are more sensitive to the combined damage of GSTO1 suppression, oxidative stress and neuroinflammation, while CA1 presents a delayed pathological response. The regional vulnerability of the hippocampus has been widely reported in neurodegenerative and brain injury models (4). Combined with our phenotypic data, the temporal sequence of APP deposition is highly consistent with the progression of cognitive deficits: the gradual accumulation of APP in the hippocampus is synchronized with the continuous decline of spatial memory retention ability, indicating that long-term oxidative and inflammatory microenvironmental disorders induced by GSTO1 dysfunction will eventually lead to structural neuronal pathological changes, which are the material basis for persistent POCD.

It is worth noting that APP deposition observed in this study reflects general neuronal damage under perioperative stress, rather than typical amyloid lesions in Alzheimer’s disease (AD)(5). Nevertheless, the similar pathological trend suggests that acute perioperative neural injury induced by GSTO1 insufficiency shares partial pathological

characteristics with chronic neurodegenerative diseases, which also provides a new perspective for the cross-research of POCD and age-related cognitive disorders(17).

4.5 Pharmacological Rationality of C1-27 In Vivo Application

In this study, we adopted C1-27, a specific covalent inhibitor of GSTO1, to construct the loss-of-function model. A notable pharmacological difference was observed between its in vitro and in vivo effective concentrations: the in vitro IC_{50} of C1-27 is at the nanomolar level, while the in vivo EC_{50} for hippocampal GSTO1 suppression reaches the millimolar range. This discrepancy is a common phenomenon in central nervous system drug delivery(18). After stereotaxic microinjection into brain parenchyma, small-molecule compounds need to overcome interstitial fluid resistance, non-specific binding to extracellular matrix proteins, cell membrane penetration barriers and rapid local metabolic clearance.

We performed a wide-range concentration gradient screening from 310 nM to 62 mM, and finally selected 3.4 mM as the working dose. Multiple verifications confirmed that this concentration could stably inhibit GSTO1 without causing obvious cytotoxicity, tissue damage or changes in animal motor function, which ensures the validity of pharmacological intervention and excludes non-specific interference caused by excessive drug concentration. Although pharmacological inhibitors may have potential off-target effects, the consistent phenotypic changes across all detection time points and indicators in this study preliminarily support that the observed cognitive, oxidative and inflammatory alterations are mainly mediated by GSTO1 suppression. Follow-up genetic intervention models including AAV-mediated knockdown and conditional knockout will further verify the target specificity.

4.6 Study Limitations and Future Perspectives

This study systematically revealed the spatiotemporal characteristics of hippocampal GSTO1 inhibition and its mediating effects on oxidative stress, neuroinflammation and neuronal pathology in aged POCD mice, and clarified the sequential pathological cascade of POCD. However, several limitations still exist. First, all conclusions are based on pharmacological inhibition of GSTO1. Although we completed rigorous dose

optimization and safety verification, potential off-target effects cannot be completely ruled out. Subsequent genetic manipulation models are required to further confirm the specific role of GSTO1. Second, we only detected classic oxidative stress indicators and the single inflammatory cytokine TNF-α, without further exploring upstream and downstream signaling pathways such as Nrf2, NF-κB and NLRP3 inflammasome which are closely related to GSTO1. The cell types (neurons, astrocytes, microglia) where GSTO1 mainly exerts its regulatory functions in the hippocampus also remain to be clarified. Third, cognitive evaluation was limited to the Morris water maze focusing on spatial learning and memory; multiple behavioral paradigms for working memory, attention and executive function should be supplemented to comprehensively assess POCD-related cognitive deficits. Fourth, only male aged mice were used in this study to avoid the interference of female cyclic hormones. Considering the sex difference in neuroinflammation and oxidative stress responses, follow-up experiments need to include female animals to improve translational value.

In conclusion, this study transforms previous clinical biomarker findings of GSTO1 into systematic in vivo mechanistic exploration. We demonstrate that hippocampal GSTO1 is a critical upstream regulator maintaining perioperative microenvironmental homeostasis. Its inhibition triggers acute oxidative burst, progressive neuroinflammation and subfield-specific neuronal pathological damage, ultimately leading to and exacerbating POCD in aged mice. The multi-stage spatiotemporal pathological cascade established in this work provides a solid preclinical basis. Targeting GSTO1 and its mediated antioxidant and anti-inflammatory pathways is expected to become a promising strategy for the prevention and treatment of perioperative neurocognitive disorders in elderly patients.

Ethics approval and consent to participate： All animal experiments in this study were reviewed and formally approved by the Laboratory Animal Welfare & Ethics Committee of Zunyi Medical University, approval number ZMU21-2207-008. All animal handling, surgical intervention and euthanasia were performed strictly in accordance with the

national guidelines for the management of laboratory animals and the ARRIVE 2.0 guidelines for reporting animal research. The original Chinese-language ethics approval certificate was uploaded as supplementary material upon initial submission. No human participants or human-derived samples were involved in this work.

Author Contributions： Guangwei Huang(G.H.) and Jing Li(J.L.) conceived and designed the study and wrote the main manuscript text. G.H., J.L. and Hualiu Chen(H.C.) performed the experiments. Huanhuan Ma(H.M.) analyzed the data and acquired funding. All authors reviewed the manuscript.

Conflict of interest： The authors declare that the research was conducted in the absence of any commercial or financial relationships that could be construed as a potential conflict of interest.

Funding: Supported by the Guizhou Provincial Science and Technology Program (No. QKH CG-LC(2025) General 079).

Data availability: The data that support the results of this study are available from the corresponding author on reasonable request.

Publisher's note： All claims expressed in this article are solely those of the authors and do not necessarily represent those of their affiliated organizations, or those of the publisher, the editors and the reviewers. Any product that may be evaluated in this article, or claim that may be made by its manufacturer, is not guaranteed or endorsed by the publisher.

References

1. Xie X, Shen Z, Hu C, Zhang K, Guo M, Wang F, et al. Dexmedetomidine Ameliorates Postoperative Cognitive Dysfunction in Aged Mice. Neurochem Res. 2021;46(9):2415-26.
2. Liu Q, Sun YM, Huang H, Chen C, Wan J, Ma LH, et al. Sirtuin 3 protects against anesthesia/surgery-induced cognitive decline in aged mice by suppressing hippocampal neuroinflammation. J Neuroinflammation. 2021;18(1):41.

3. Xu Y, Bankhead A, 3rd, Tian X, Tang J, Ljungman M, Neamati N. Deletion of Glutathione S-Transferase Omega 1 Activates Type I Interferon Genes and Downregulates Tissue Factor. Cancer Res. 2020;80(17):3692-705.
4. Piacentini S, Polimanti R, Squitti R, Mariani S, Migliore S, Vernieri F, et al. GSTO1*E155del polymorphism associated with increased risk for late-onset Alzheimer's disease: association hypothesis for an uncommon genetic variant. Neurosci Lett. 2012;506(2):203-7.
5. Jia Y, Gao MD, Liu YF, Lu L, Chen G, Chen Y. Genetic dissection of glutathione S-transferase omega-1: identification of novel downstream targets and Alzheimer's disease pathways. Neural Regen Res. 2022;17(11):2452-8.
6. Ma H, Wei Y, Chen W, Chen S, Wang Y, Cao S, et al. Serum proteomics study on cognitive impairment after cardiac valve replacement surgery: a prospective observational study. PeerJ. 2024;12:e17536.
7. Rout M, Prusty SK, Singh V, Kispotta S, Sarangi P, Kar DM. Targeting the Microbiota-Gut-Brain Axis: Bacillus coagulans Protects Against Rotenone-Induced Parkinson's Disease in Rats. Neurochem Res. 2026;51(2).
8. Ramkumar K, Samanta S, Kyani A, Yang S, Tamura S, Ziemke E, et al. Mechanistic evaluation and transcriptional signature of a glutathione S-transferase omega 1 inhibitor. Nat Commun. 2016;7:13084.
9. Zhao Z, Sun C, Liu X, Yu P, Wang Y, Li H, et al. GSTO1 Promotes Cell Proliferation and Stemness of Cervical Cancer via Activating PI3K/AKT/mTOR Pathway. FASEB J. 2026;40(7):e71702.
10. Zhang X, Lu Q, Meng X, Kim JY. Protocol to induce neurodegeneration in a local area of the mouse brain by stereotaxic injection. STAR Protoc. 2024;5(3):103243.
11. Podbielska M, Kus-Liśkiewicz M, Płoch D, Szpyrka EJM. Co-Exposure to Glyphosate and Polyethylene Microplastic Affects Their Toxicity to Chlorella vulgaris: Implications for Algal Health and Aquatic Risk. 2025;30(19):3972.
12. Khallaf WAI, Messiha BAS, Abo-Youssef AMH, El-Sayed NS. Protective effects of telmisartan and tempol on lipopolysaccharide-induced cognitive impairment, neuroinflammation, and amyloidogenesis: possible role of brain-derived neurotrophic factor. Can J Physiol Pharmacol. 2017;95(7):850-60.
13. Hindam MO, Ahmed LA, El Sayed NS, Khattab M, Sallam NA. Repositioning of baricitinib for management of memory impairment in ovariectomized/D-galactose treated rats: A potential role of JAK2/STAT3-PI3K/AKT/mTOR signaling pathway. Life Sci. 2024;351:122838.
14. Sayed NS, Abidar S, Nhiri M, Hritcu L, Ibrahim WWJPR. Aqueous extract of Ceratonia siliqua L. leaves elicits antioxidant, anti-inflammatory, and AChE inhibiting effects in amyloid-β42-induced cognitive deficit mice: Role of α7-nAChR in modulating Jak2/PI3K/Akt/GSK-3β/β-catenin cascade. 2023;37(6):2437-53.
15. Sirwi A, Sayed NS, Abdallah HM, Ibrahim SRM, Mohamed GA, El-Halawany AM, et al. Umuhengerin Neuroprotective Effects in Streptozotocin-Induced Alzheimer's Disease Mouse Model via Targeting Nrf2 and NF-Kβ Signaling Cascades. 2021;10(12):2011.
16. Qiu LL, Ji MH, Zhang H, Yang JJ, Sun XR, Tang H, et al. NADPH oxidase 2-derived reactive oxygen species in the hippocampus might contribute to microglial activation in postoperative cognitive dysfunction in aged mice. Brain Behav Immun. 2016;51:109-18.
17. Wang H, Tu J, Zhang J, Wang W, Yuan Z, Li C, et al. Integrated multi-omics profiling reveals shared mechanistic pathways in asthma-allergic rhinitis comorbidity: A hybrid machine learning framework leveraging Mendelian randomization for precision diagnostics. World Allergy Organ J. 2025;18(10):101120.
18. Kim K, Choi J, Iram S, Kim J. Regulation of Glutathione S-Transferase Omega 1 Mediated by Cysteine Residues Sensing the Redox Environment. Int J Mol Sci. 2024;25(10).
19. Zhang Z, Yang W, Wang L, Zhu C, Cui S, Wang T, et al. Unraveling the role and mechanism of mitochondria in postoperative cognitive dysfunction: a narrative review. J Neuroinflammation. 2024;21(1):293.
20. Gascoigne DA, Minhaj MM, Aksenov DP. Neonatal Anesthesia and Oxidative Stress. Antioxidants (Basel). 2022;11(4).

21. Board PG, Menon D. Structure, function and disease relevance of Omega-class glutathione transferases. Arch Toxicol. 2016;90(5):1049-67.
22. Lee JM, Lee JH, Song MK, Kim YJ. NXP032 Ameliorates Aging-Induced Oxidative Stress and Cognitive Impairment in Mice through Activation of Nrf2 Signaling. Antioxidants (Basel). 2022;11(1).
23. Lee JM, Lee JH, Song MK, Kim YJ. NXP031 Improves Cognitive Impairment in a Chronic Cerebral Hypoperfusion-Induced Vascular Dementia Rat Model through Nrf2 Signaling. Int J Mol Sci. 2021;22(12).
24. Aremu PA, Ajayi AM, Ben-Azu B, Orewole OT, Umukoro S. Spinal and general anesthesia produces differential effects on oxidative stress and inflammatory cytokines in orthopedic patients. Drug Metab Pers Ther. 2020.
25. Ercan H, Reumiller CM, Muhlberger J, Hsu F, Schmidt GJ, Umlauf E, et al. Platelets mirror changes in the frontal lobe antioxidant system in Alzheimer's disease. Alzheimers Dement. 2025;21(4):e70117.
26. Hughes MM, Hooftman A, Angiari S, Tummala P, Zaslona Z, Runtsch MC, et al. Glutathione Transferase Omega-1 Regulates NLRP3 Inflammasome Activation through NEK7 Deglutathionylation. Cell Rep. 2019;29(1):151-61 e5.
27. Piaggi S, Marchi E, Carnicelli V, Zucchi R, Griese M, Hector A, et al. Airways glutathione S-transferase omega-1 and its A140D polymorphism are associated with severity of inflammation and respiratory dysfunction in cystic fibrosis. J Cyst Fibros. 2021;20(6):1053-61.
28. Shen NX, Luo MY, Gu WM, Gong M, Lei HM, Bi L, et al. GSTO1 aggravates EGFR-TKIs resistance and tumor metastasis via deglutathionylation of NPM1 in lung adenocarcinoma. Oncogene. 2024;43(33):2504-16.
29. Deepthi M, Rebecca C, Luke A J ON, Philip G BJJCS. GSTO1-1 modulates metabolism in macrophages activated through the LPS and TLR4 pathway. 2015;128(10).
30. Gao K, Wu Y, Zhang Y, Dang P, Xue H, Li T, et al. Alpha-lipoic acid alleviates oxidative stress and brain damage in patients with sevoflurane anesthesia. Front Pharmacol. 2025;16:1572156.
31. Cha SJ, Lee S, Choi HJ, Han YJ, Jeon YM, Jo M, et al. Therapeutic modulation of GSTO activity rescues FUS-associated neurotoxicity via deglutathionylation in ALS disease models. Dev Cell. 2022;57(6):783-98 e8.

Figure 1. CTB fluorescence distribution in the hippocampus confirming injection site localization.

Figure 2. GSTO1 protein expression in the hippocampus after treatment with different concentrations of C1-27.

Note: Group 1: 310 nM; Group 2: 3.1 μM; Group 3: 31 μM; Group 4: 310 μM; Group 5: 3.1 mM; Group 6: 31 mM; Group 7: 62 mM; Control group: DMSO(10%).

Figure 3. Four-parameter logistic (4PL) regression curve illustrating the dose-dependent inhibitory effect of C1-27 on hippocampal GSTO1 protein expression.

Note: Data were fitted with the four-parameter logistic model (y=(A-D)/[1+(x/C)^B]+D) using ELISA Calc software. Fitted parameters were (A=8.31817), (B=-1.93028), (C=0.17129), (D=-1.69717), and (R^2=0.96104).
X-axis: GSTO1 inhibition rate; Y-axis: logarithmic value of C1-27 concentration.

Figure 4. Morris water maze navigation task results for each group of mice.

*Note: A – Escape latency over 5 days of training for each group. B – Total distance traveled by each group; *P < 0.05 vs Day 1; #P < 0.05 vs Day 2; &P < 0.05 vs Day 3.*

Figure 5. Morris water maze probe trial results for spatial memory assessment.

*Note: (A) Platform crossing counts; (B) Percentage of swimming distance in the target quadrant; (C) Percentage of swimming time in the target quadrant. Statistics: one-way ANOVA with Tukey's post-hoc test. ns, not significant; *P < 0.05, **P < 0.01, ***P < 0.001.*

Figure 6. Western blot detection and quantification of GSTO1 protein at postoperative 6 h, 3 days and 7 days.

*Note: (A) Original blot images of GSTO1 (28 kDa) and GAPDH (36 kDa). (B) Statistical quantification of normalized GSTO1 expression. One-way ANOVA with Tukey's post-hoc test. *P < 0.05, **P < 0.01, ***P < 0.001.*

Figure 7. ELISA quantification of hippocampal oxidative stress biomarkers at postoperative 6 h, 3 days and 7 days.

*Note: (A) GSH concentration; (B) GSSG concentration; (C) GSH/GSSG ratio; (D) MDA content; (E) ROS activity. Statistics: one-way ANOVA with Tukey's post-hoc test. *P < 0.05, **P < 0.01, ***P < 0.001.*

Figure 8. Immunofluorescence detection and quantification of GSTO1 and TNF-α in hippocampal CA1 area.

*Note: (A) Representative staining images (DAPI, GSTO1, TNF-α, Merge) at 6 h, 3 d and 7 d post-modeling, scale bar = 40 μm. (B) Relative fluorescence intensity of GSTO1. (C) Relative fluorescence intensity of TNF-α. One-way ANOVA with Tukey's post-hoc test. ns, no significance; *P < 0.05, **P < 0.01, ***P < 0.001.*

Figure 9. Immunohistochemical detection and quantification of APP expression in mouse hippocampal CA1, CA3 and DG subregions.

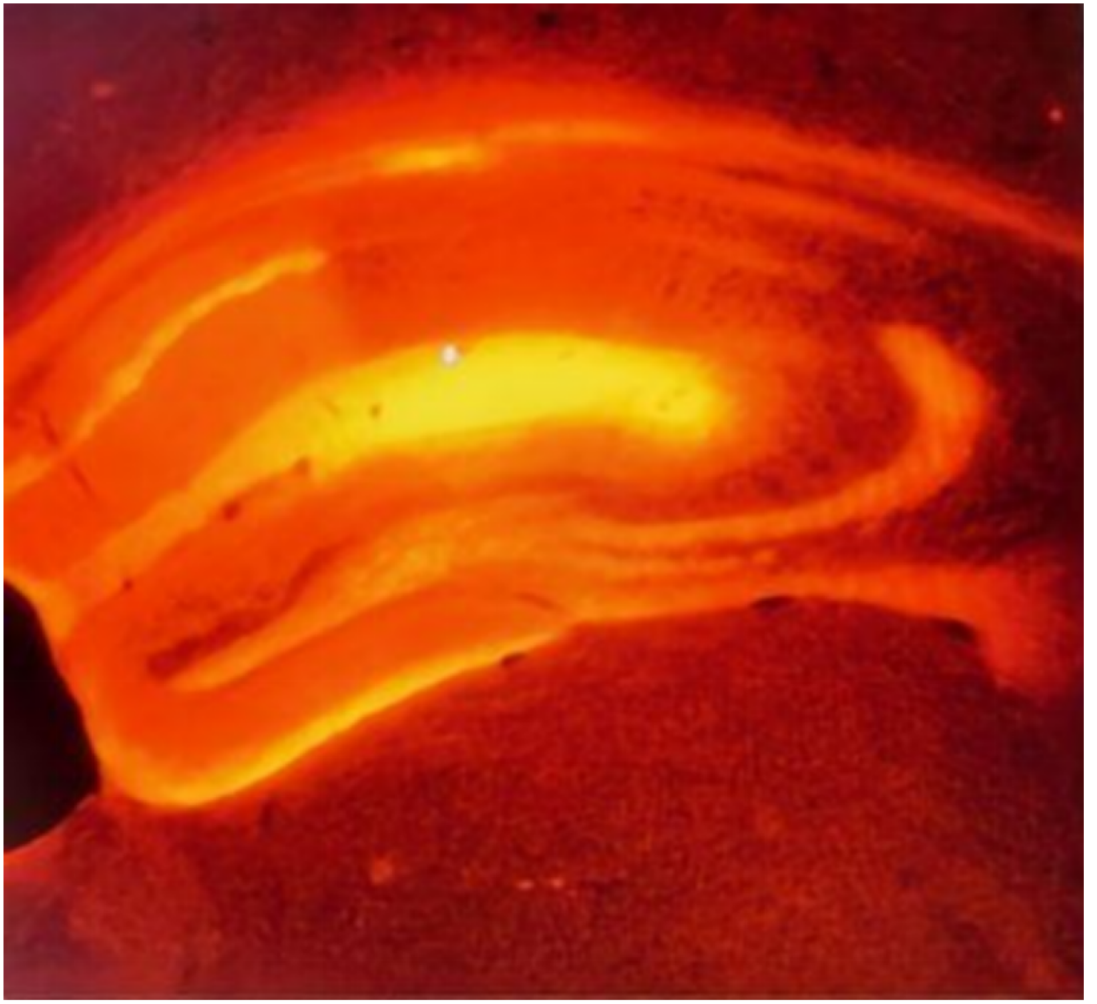
*Note: (A–C) Representative IHC images of APP at postoperative 6 h, 3 days and 7 days, scale bar = 40 μm. (D–F) Statistical comparison of APP average optical density (AOD) in corresponding subregions. One-way ANOVA with Tukey's post-hoc test. ns, no significance; *P < 0.05, **P < 0.01, ***P < 0.001.*

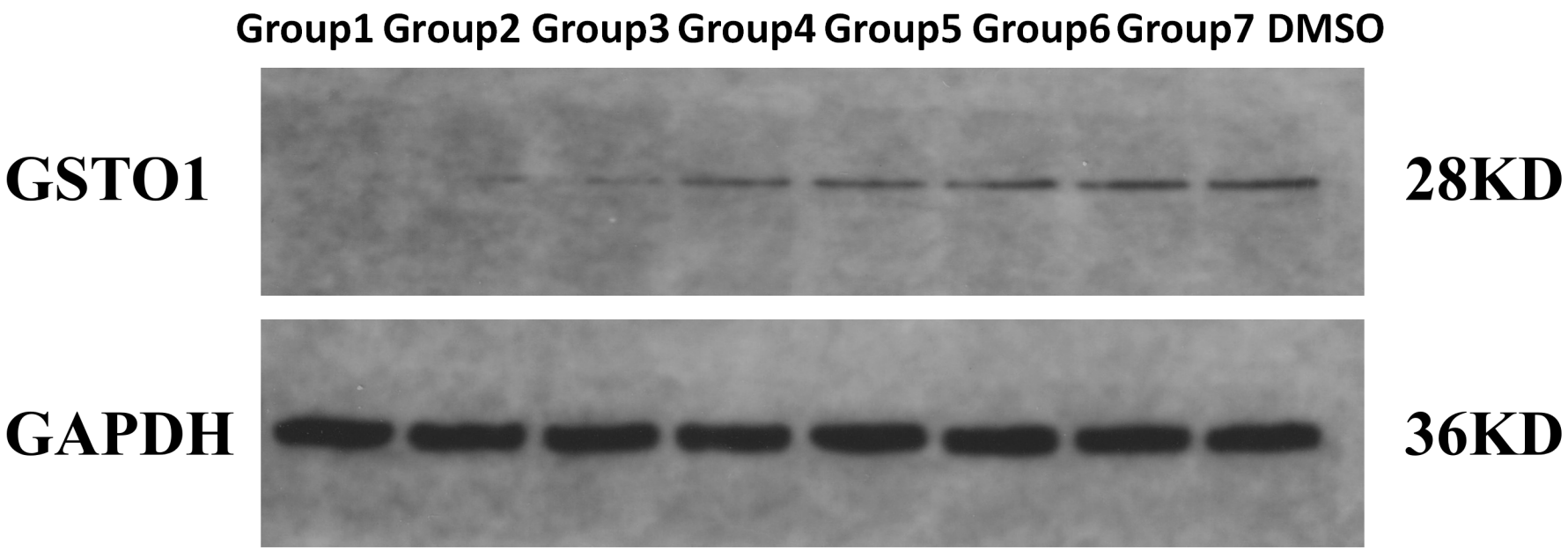
Table 1. C1-27 concentration gradient settings in the hippocampus

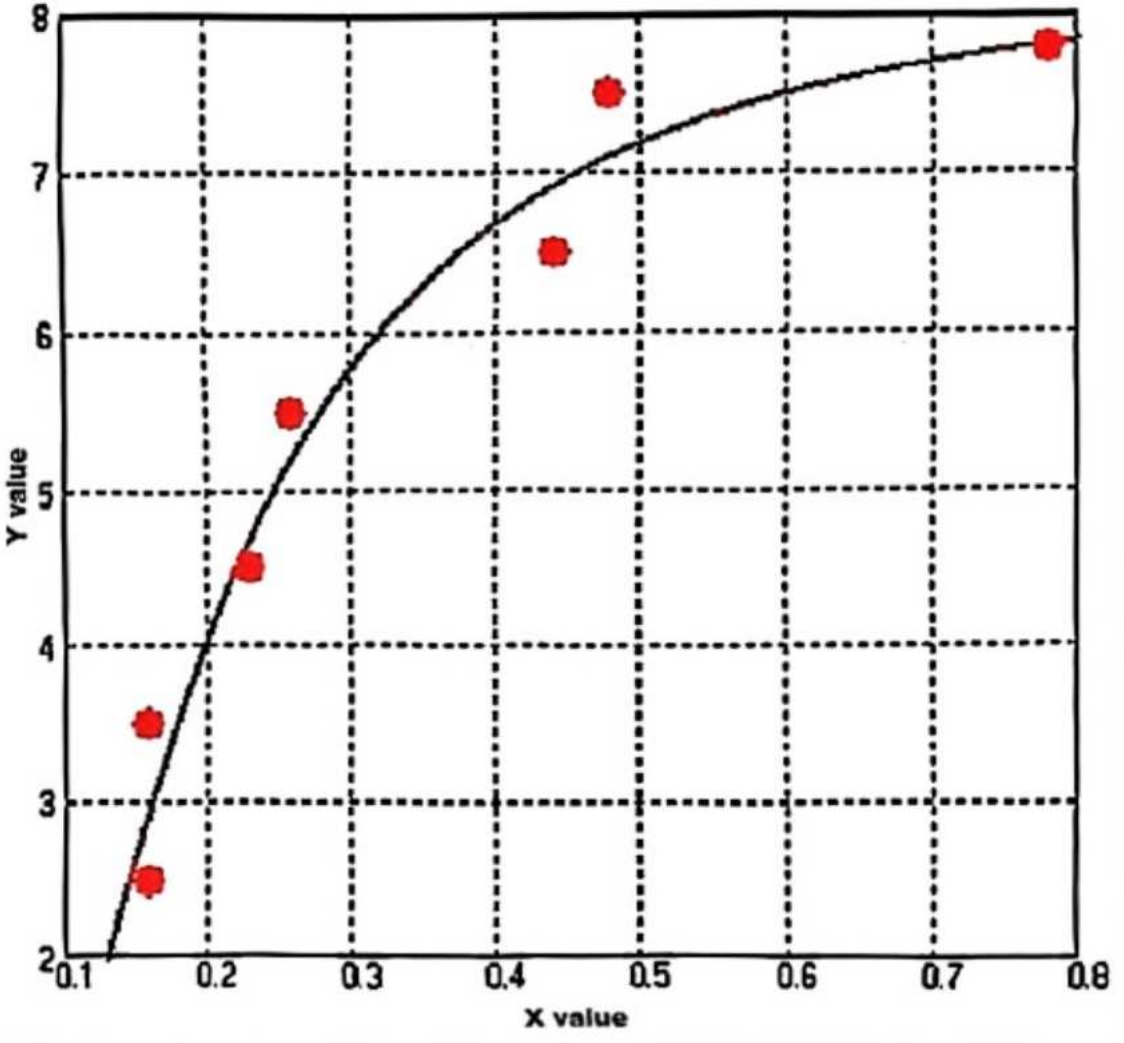
Group	C57BL/6 mice (n)	Injection reagent	Concentration	Dose	Method
Group 1	2	C1-27	310 nM	1.2 μL	Stereotactic hippocampal injection
Group 2	2	C1-27	3.1 μM	1.2 μL	Stereotactic hippocampal injection
Group 3	2	C1-27	31 μM	1.2 μL	Stereotactic hippocampal injection
Group 4	2	C1-27	310 μM	1.2 μL	Stereotactic hippocampal injection
Group 5	2	C1-27	3.1 mM	1.2 μL	Stereotactic hippocampal injection
Group 6	2	C1-27	31 mM	1.2 μL	Stereotactic hippocampal injection
Group 7	2	C1-27	62 mM	1.2 μL	Stereotactic hippocampal injection
Control	2	DMSO (10%)	–	1.2 μL	Stereotactic hippocampal injection

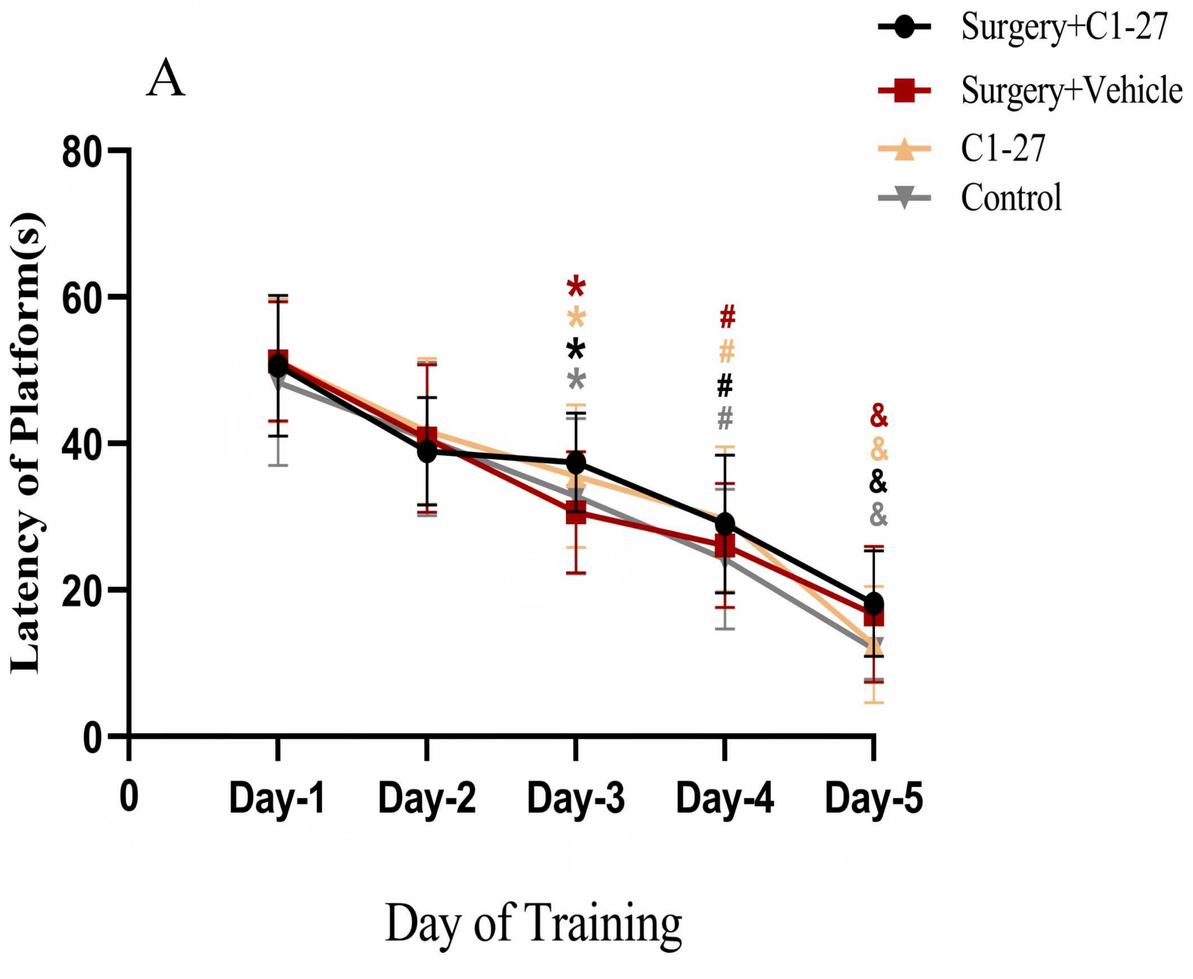
Table 2. ELISA measurement of GSTO1 OD values and inhibition rates

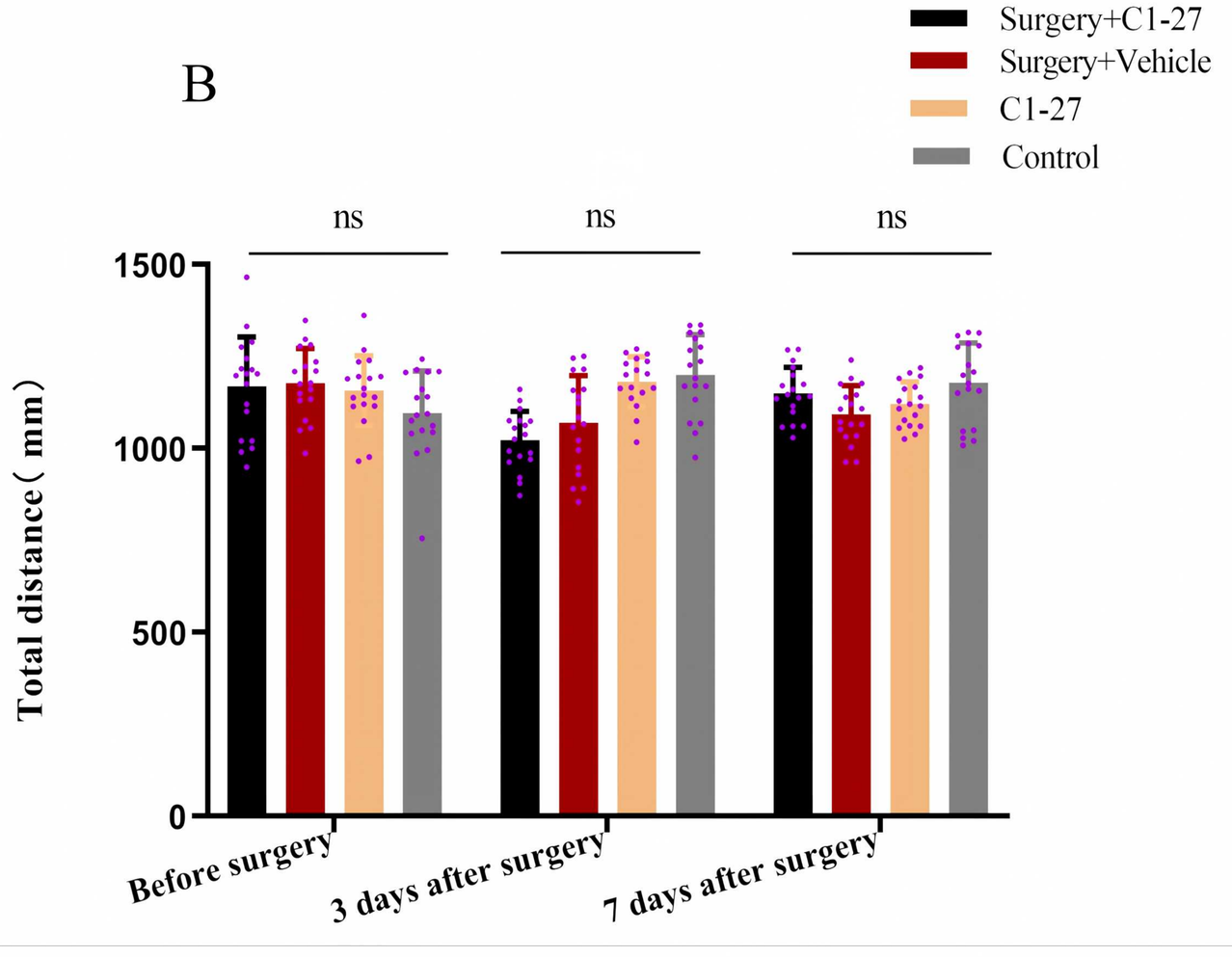
Group	C1-27 concentration	OD_1	OD_2	Average OD	Inhibition rate
Control (n=2)	DMSO(%)	0.83	0.89	0.86	–
Group 1 (n=2)	310 nM	0.73	0.72	0.725	0.16
Group 2 (n=2)	3.1 μM	0.74	0.71	0.725	0.16
Group 3 (n=2)	31 μM	0.68	0.65	0.665	0.23
Group 4 (n=2)	310 μM	0.64	0.63	0.635	0.26
Group 5 (n=2)	3.1 mM	0.50	0.47	0.485	0.44
Group 6 (n=2)	31 mM	0.46	0.44	0.450	0.48
Group 7 (n=2)	62 mM	0.20	0.10	0.150	0.78



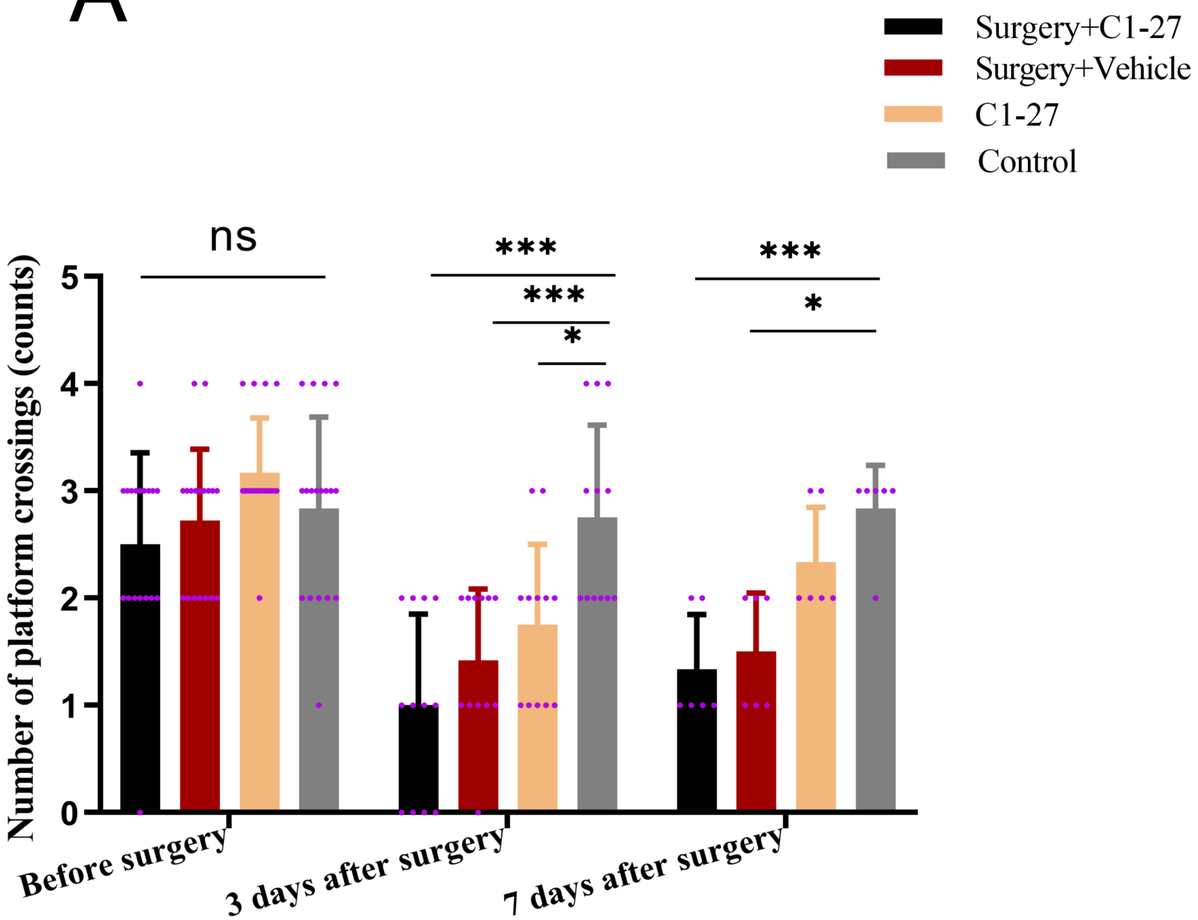

Group1 Group2 Group3 Group4 Group5 Group6 Group7 DMSO
GSTO1
28KD
GAPDH
36KD


8
7
6
5
4
3
2
Y value
0.1
0.2
0.3
0.4
0.5
0.6
0.7
0.8
X value

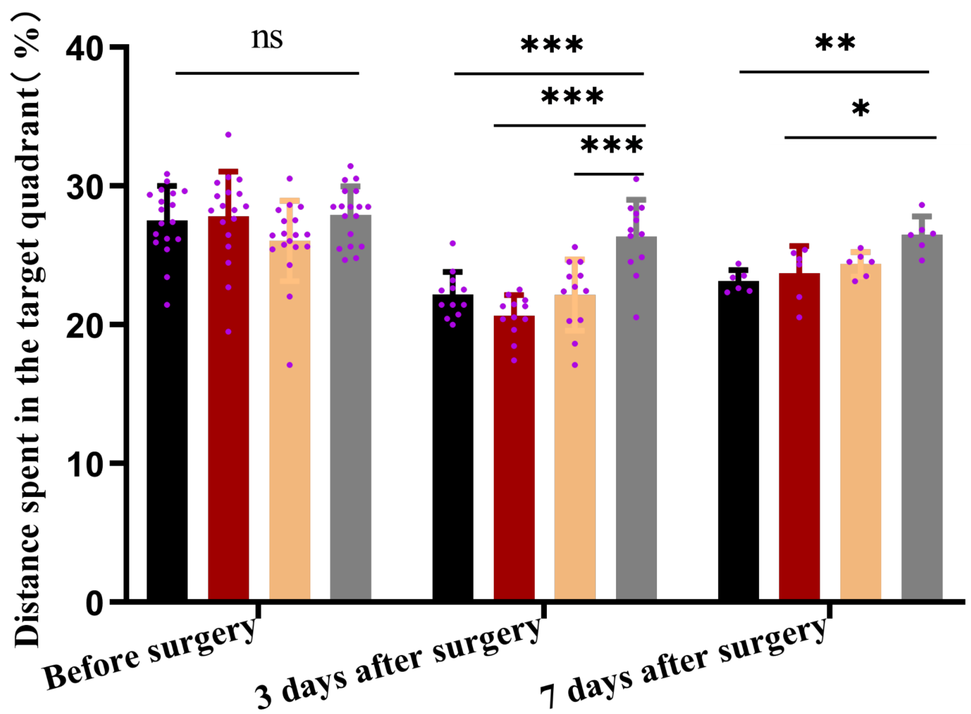

A
Surgery+C1-27
Surgery+Vehicle
C1-27
Control
Latency of Platform(s)
80
60
40
20
0
0
Day-1
Day-2
Day-3
Day-4
Day-5
Day of Training


B
Surgery+C1-27
Surgery+Vehicle
C1-27
Control
ns
ns
ns
Total distance（mm）
1500
1000
500
0
Before surgery
3 days after surgery
7 days after surgery

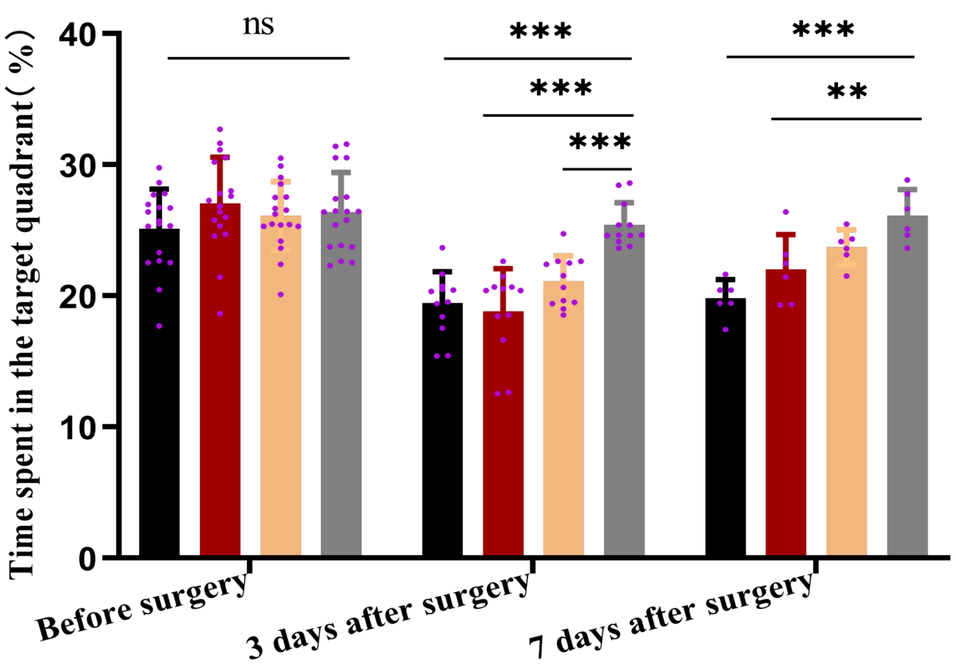
A

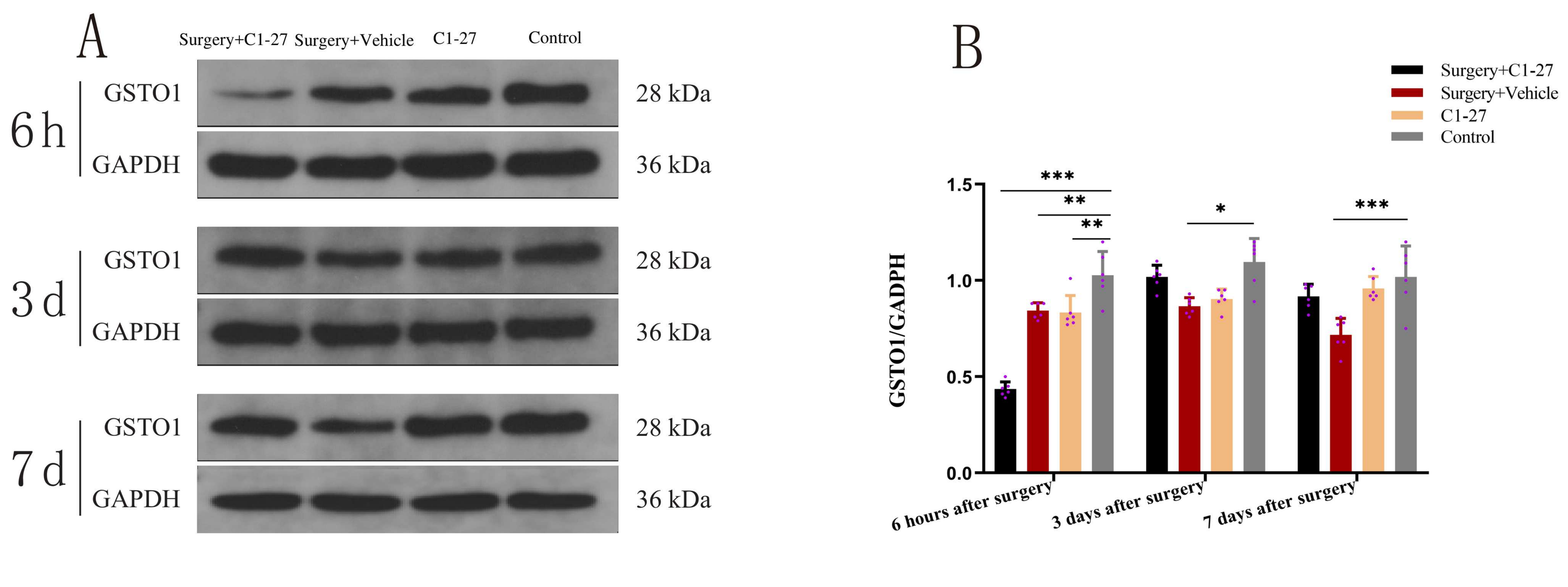

Surgery+C1-27
Surgery+Vehicle
C1-27
Control
Number of platform crossings (counts)
0
1
2
3
4
5
ns
***
***
*
***
*
Before surgery
3 days after surgery
7 days after surgery

B

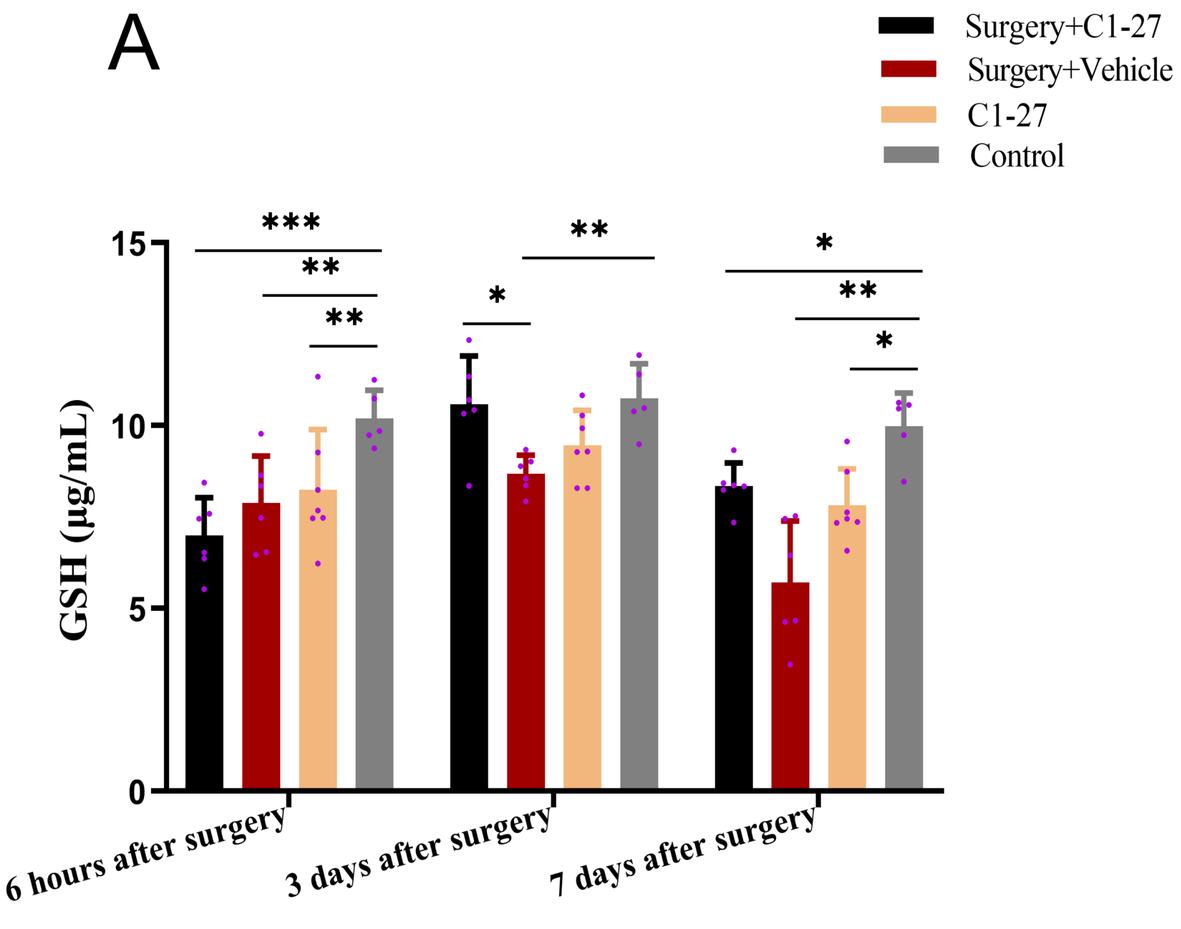

Distance spent in the target quadrant(%)
0
10
20
30
40
ns
***
***
***
**
*
Before surgery
3 days after surgery
7 days after surgery

C

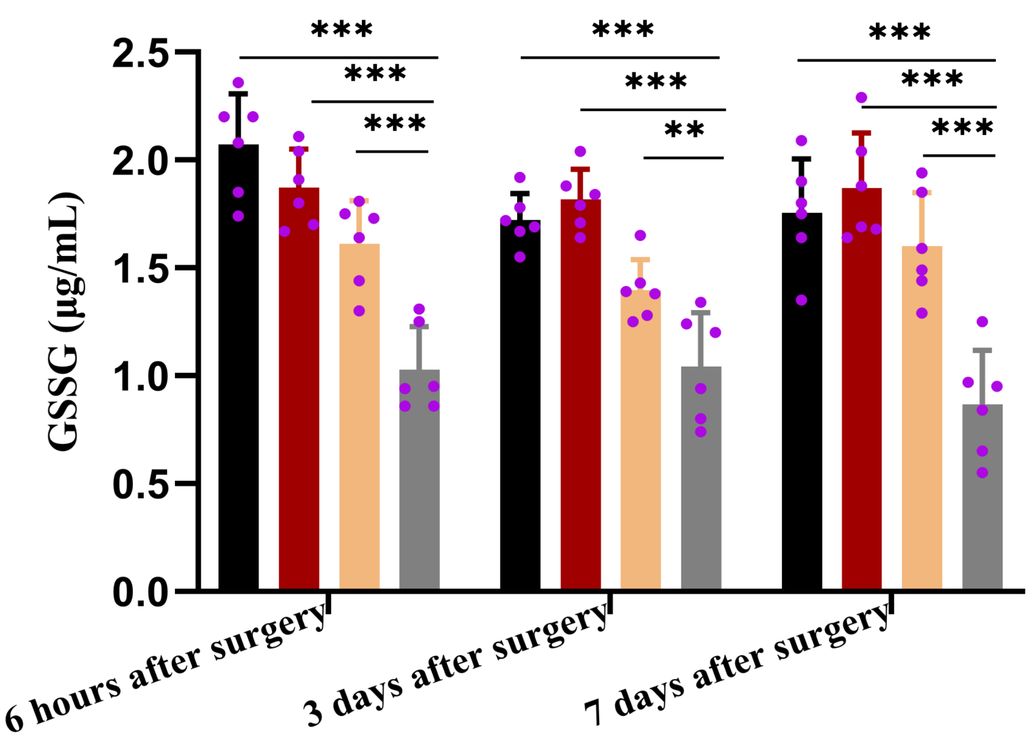

Time spent in the target quadrant(%)
0
10
20
30
40
ns
***
***
***
***
**
Before surgery
3 days after surgery
7 days after surgery


A
Surgery+C1-27
Surgery+Vehicle
C1-27
Control
6 h
GSTO1
28 kDa
GAPDH
36 kDa
3 d
GSTO1
28 kDa
GAPDH
36 kDa
7 d
GSTO1
28 kDa
GAPDH
36 kDa
B
Surgery+C1-27
Surgery+Vehicle
C1-27
Control
GSTO1/GADPH
1.5
1.0
0.5
0.0
***
**
**
*
***
6 hours after surgery
3 days after surgery
7 days after surgery

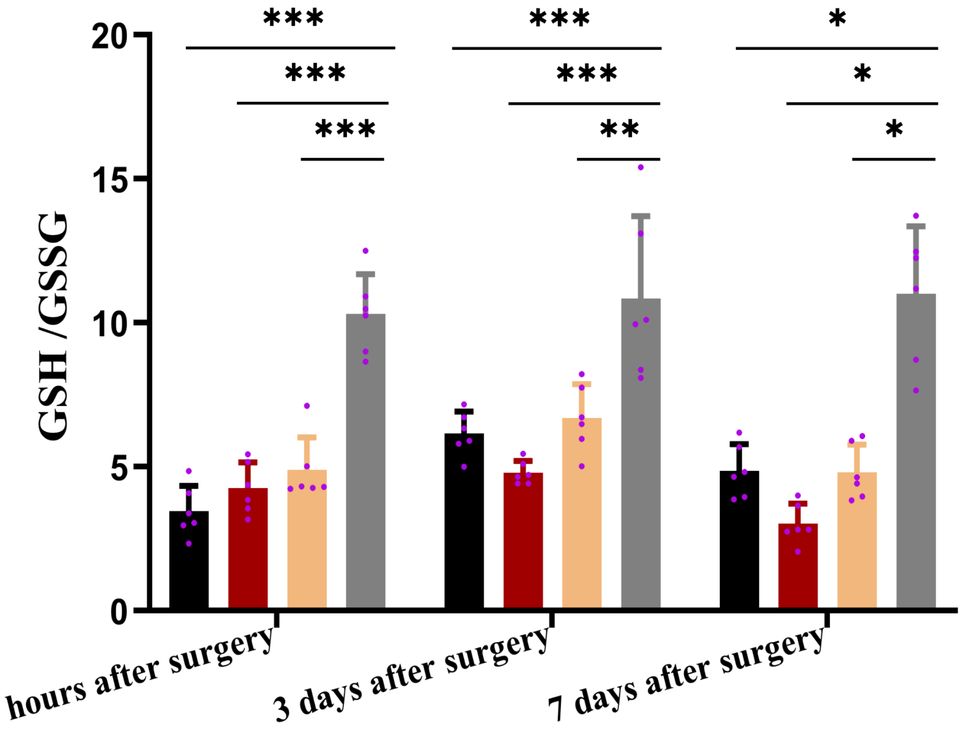
A


Surgery+C1-27
Surgery+Vehicle
C1-27
Control
GSH (μg/mL)
15
10
5
0
***
**
**
*
**
*
*
**
*
6 hours after surgery
3 days after surgery
7 days after surgery

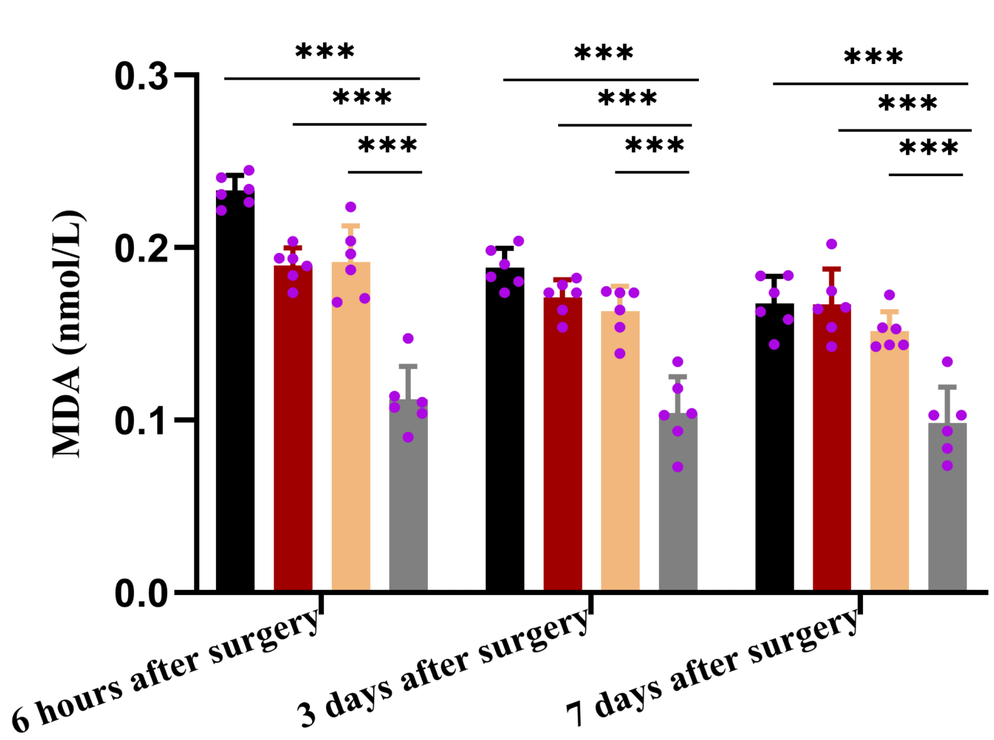
B


GSSG (μg/mL)
2.5
2.0
1.5
1.0
0.5
0.0
***
***
***
***
***
**
***
***
***
6 hours after surgery
3 days after surgery
7 days after surgery

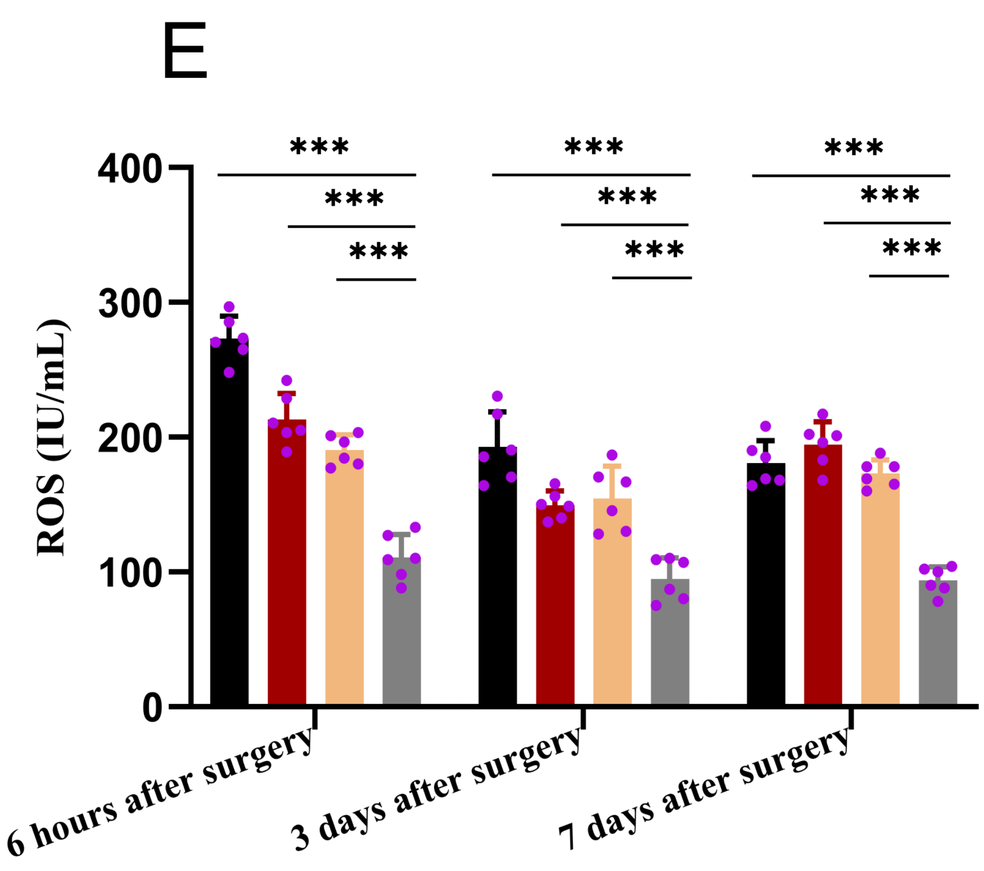
C


GSH /GSSG
20
15
10
5
0
***
***
***
***
***
**
*
*
*
6 hours after surgery
3 days after surgery
7 days after surgery

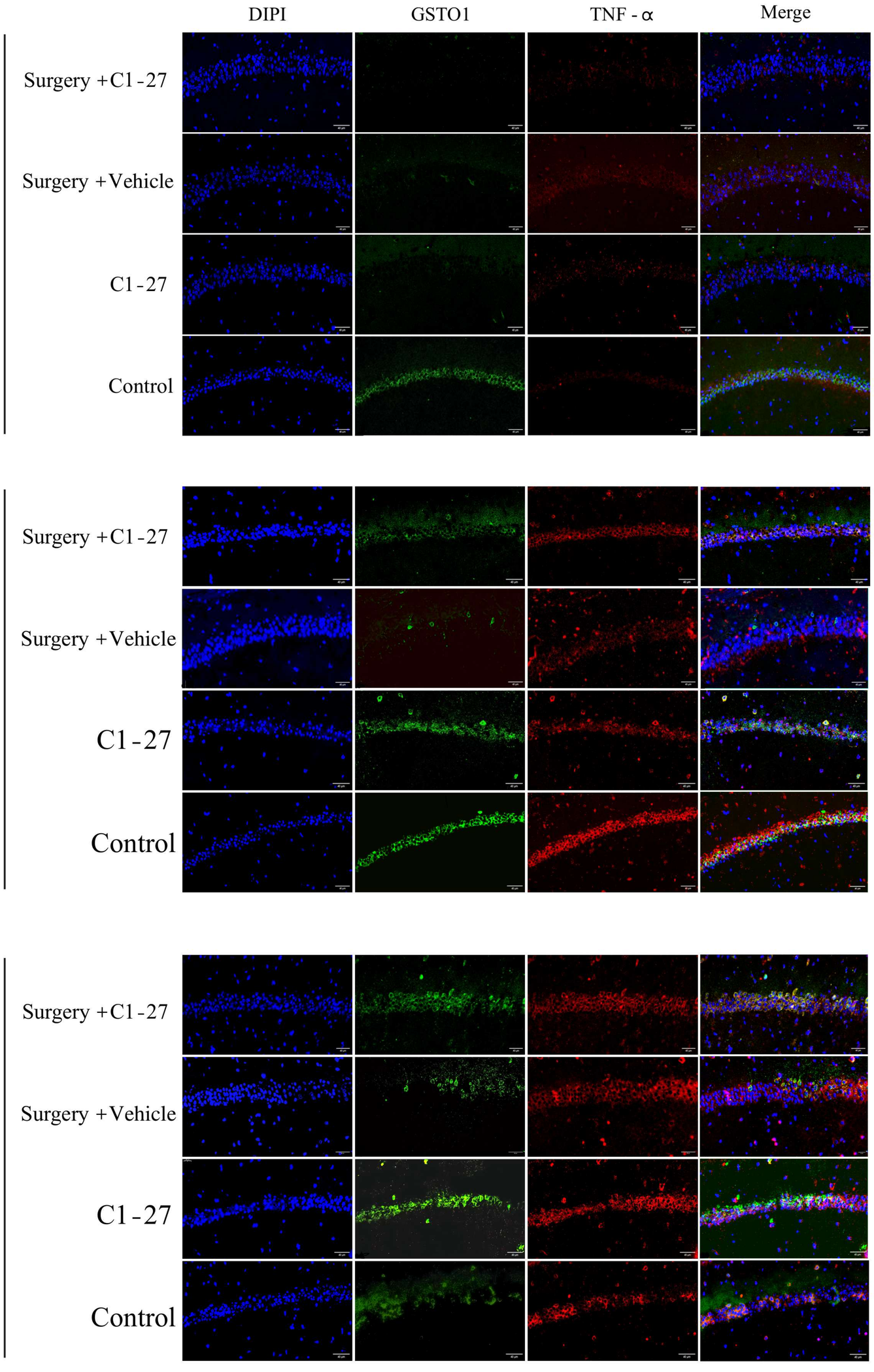
D


MDA (nmol/L)
0.3
0.2
0.1
0.0
***
***
***
***
***
***
***
***
***
6 hours after surgery
3 days after surgery
7 days after surgery

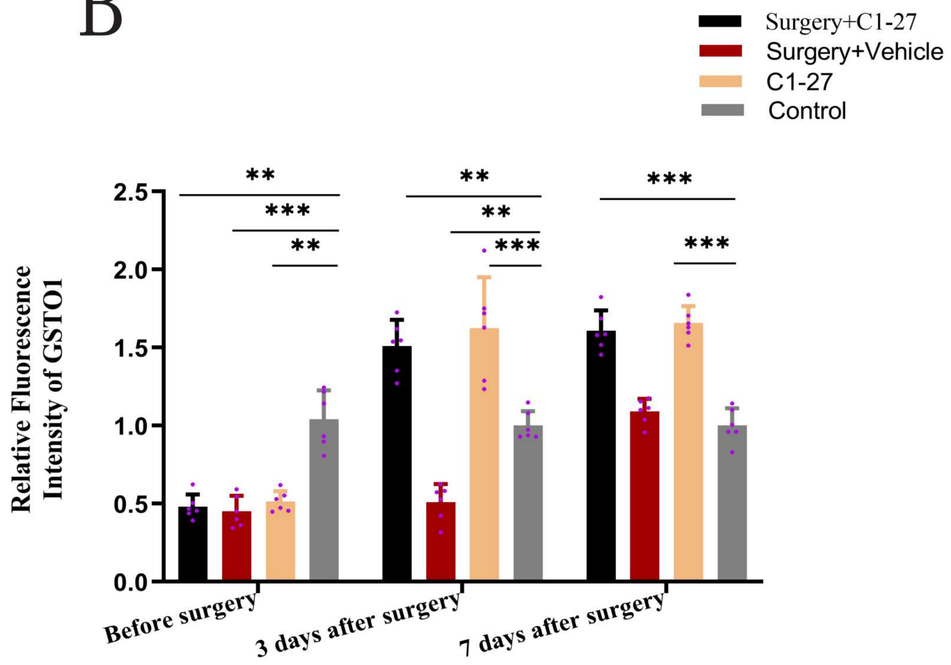
E


ROS (IU/mL)
400
300
200
100
0
***
***
***
***
***
***
***
***
***
6 hours after surgery
3 days after surgery
7 days after surgery

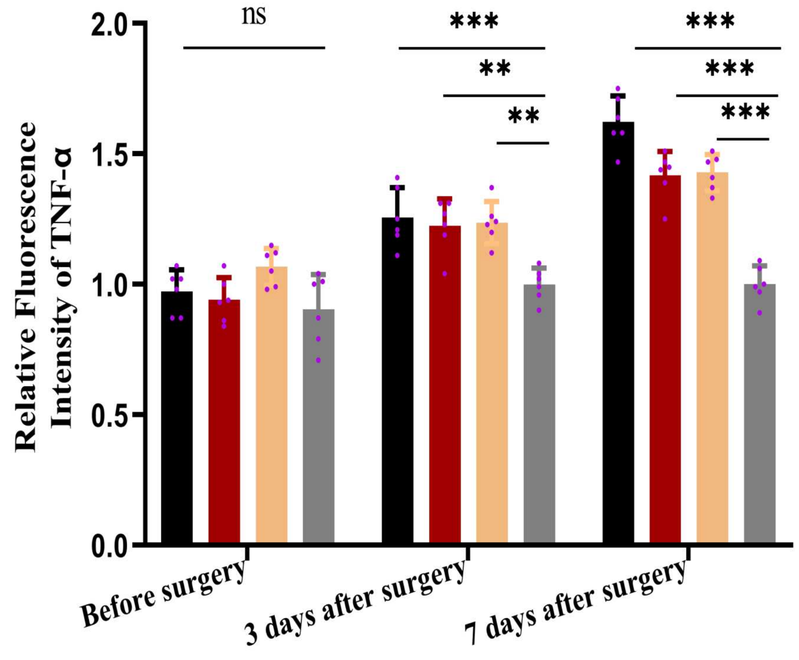
A


DIPI
GSTO1
TNF - α
Merge
6h
Surgery +C1 -27
Surgery +Vehicle
C1 -27
Control
3d
Surgery +C1 -27
Surgery +Vehicle
C1 -27
Control
7d
Surgery +C1 -27
Surgery +Vehicle
C1 -27
Control

B


Surgery+C1-27
Surgery+Vehicle
C1-27
Control
Relative Fluorescence Intensity of GSTO1
2.5
2.0
1.5
1.0
0.5
0.0
**
***
**
**
***
**
***
***
Before surgery
3 days after surgery
7 days after surgery

C


Relative Fluorescence Intensity of TNF-α
2.0
1.5
1.0
0.5
0.0
ns
***
**
**
***
***
***
Before surgery
3 days after surgery
7 days after surgery

Surgery+C1-27 | Surgery+Vehicle | C1-27 | Control

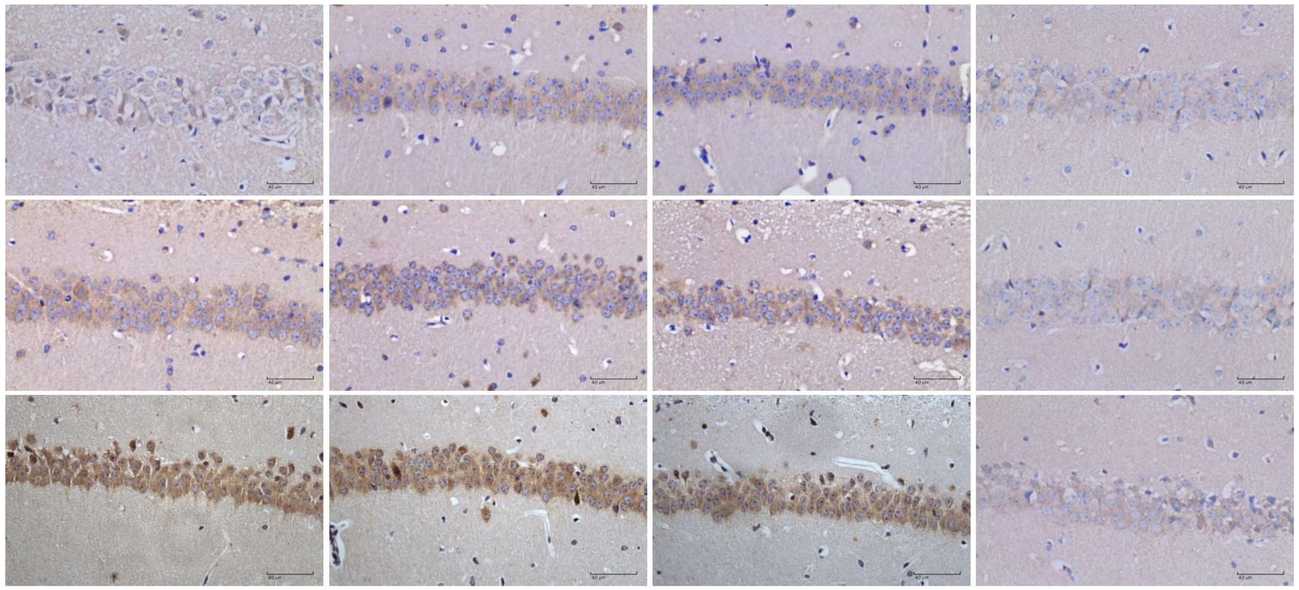
A

CA1

6h

3d

7d



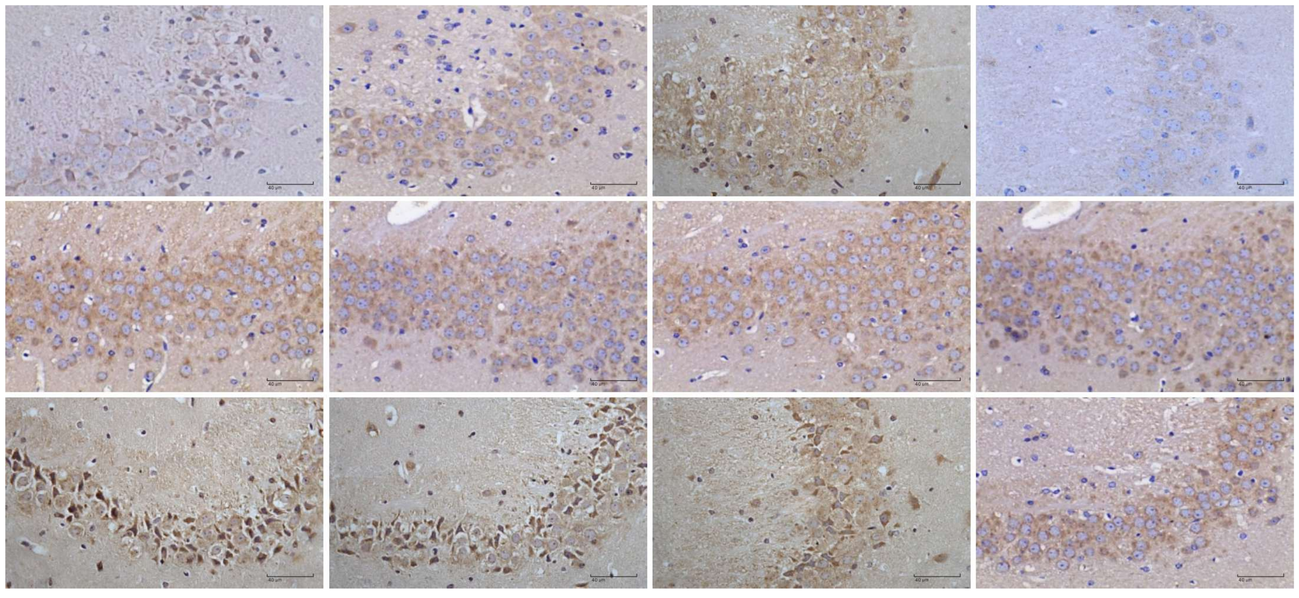
B

CA3

6h

3d

7d



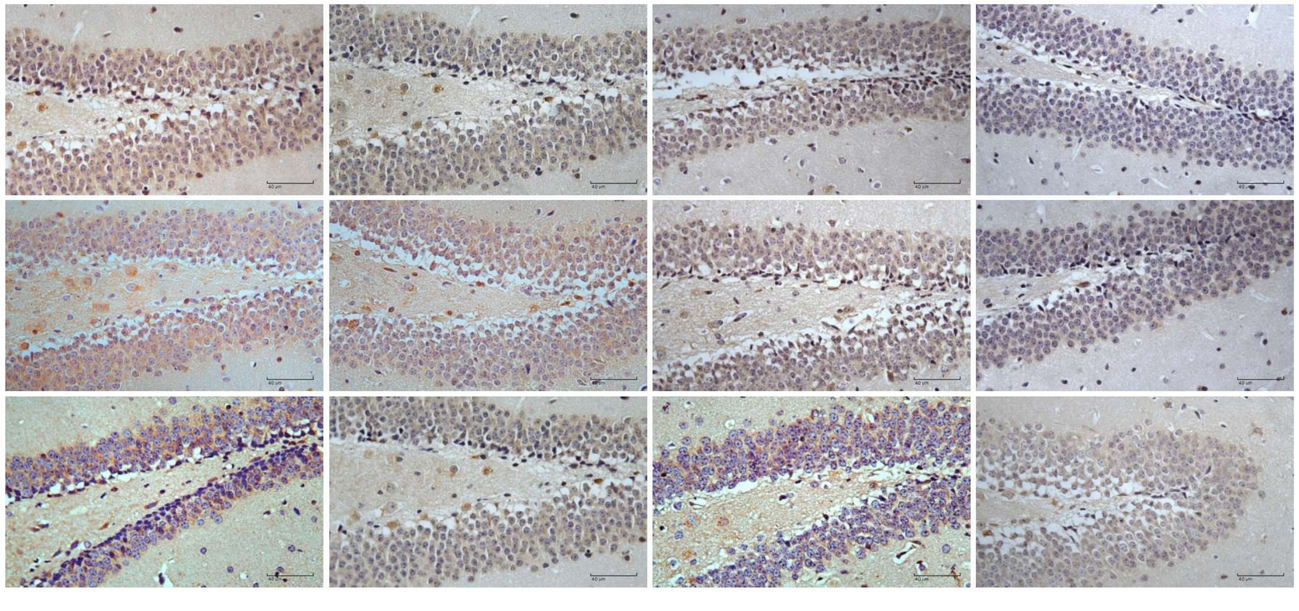
C

DG

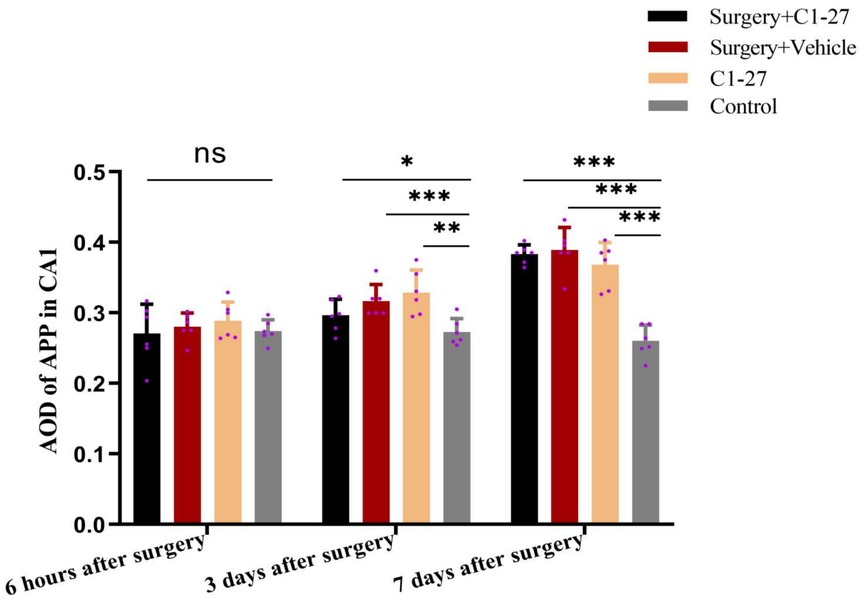
6h

3d

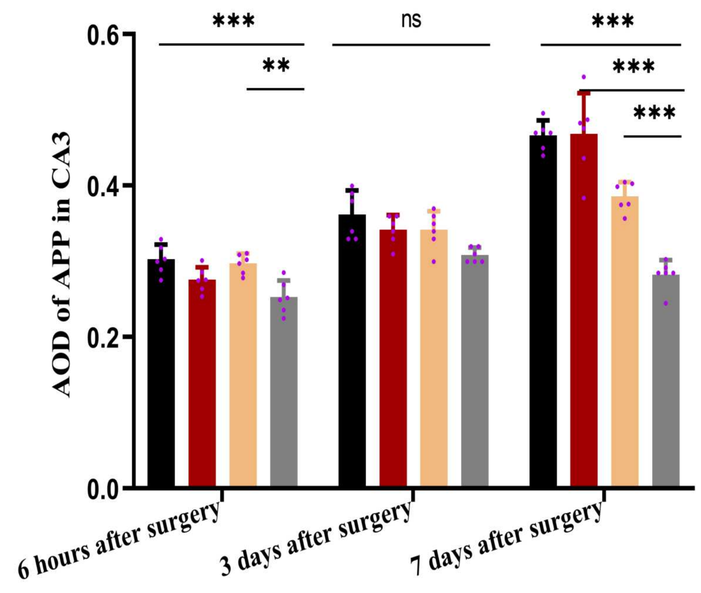
7d



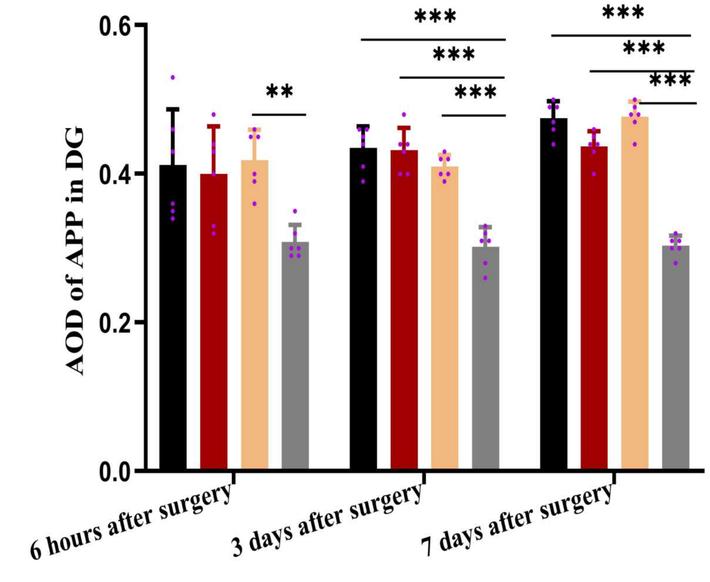
D



E



F



Supplementary Files

This is a list of supplementary files associated with this preprint. Click to download.

- SupplementaryInformationNote.pdf
- WBimages.pdf
- TablesS1S3.xlsx
- TableS4WBGrayscaleValue.xlsx
- TableS5WBRelativeExpression.xlsx